A LOW COST PLANAR NEAR-FIELD / FAR-FIELD ANTENNA MEASUREMENT SYSTEM

BING YAN

A Low Cost Planar Near-Field / Far-Field Antenna Measurement System

By

© Bing Yan

A thesis submitted to the School of Graduate Studies

in partial fulfillment of the requirements for the degree of

Master of Engineering

Faculty of Engineering and Applied Science

Memorial University of Newfoundland

Septmber, 1997

St. John's Newfoundland Canada

Abstract

In this thesis, a low cost planar near-field/far-field (NF/FF) antenna measurement system is designed, built and validated in Center for Cold Ocean Research Engineering (C-CORE), Memorial University of Newfoundland. The design of the system is presented in detail, a faster technique is used to speed the determination of the far-field radiation pattern. The basic theory of near-field antenna measurements is reviewed. A software package has been designed which has a user friendly interface. Details of the NF/FF transformation using fourier transform are presented. Far-field radiation patterns calculated from near-field measurements have been compared with the far-field patterns measured directly inside C-CORE's RF anechoic chamber, and reasonably accurate results are observed for a number of antennas. Based on the cost of the system ($2,000), the reasonably accurate results are quite acceptable. This NF/FF measurement system is an addition to the Memorial University electromagnetic measurement facility.

Acknowledgment

I would like to express my deepest gratitude to my supervisors Dr. B.P. Sinha and Dr. S. A. Saoudy. Without their stimulating my interest in this exciting field and their constant encouragement and guidance throughout the research, this thesis would not have been possible.

I would like to thank C-CORE, Memorial University of Newfoundland, for providing the electromagnetic facility, help and dedication of their employees especially Dr. S. A. Saoudy who is a senior electromagnetic engineer at C-CORE.

The financial support by Natural Sciences and Engineering Research Council of Canada, the Faculty of Engineering and Applied Science of memorial University, is gratefully acknowledged.

The last but not the least, I would also like to thank my parents Mr. Zhi Yan and Ms. Dongzhi Li for a joyful dawning in the quest for truth and knowledge.

Contents

Abstract ii

Acknowledgment iii

List of Figures vii

List of Tables ix

1 Introduction 1

1.1 Statement of the problem 1

1.2 Research Background 2

1.3 Scope of the work 3

1.4 Organization of the thesis 4

2 Literature Review 6

2.1 Definition of near-field and far-field 6

2.2 Near-field measurement concepts 8

2.3 Advantage of near-field measurement 11

2.4 Some near-field antenna measurement criteria 12

2.4.1 Spacing criteria 12

2.4.2 Distance criteria 12

2.5 Algorithms used 13

2.6 Validation 14

2.7 Planar near-field measurement 16

2.7.1 Near-field sampling 17

2.7.2 Rectangular-planar near-field measurement 18

2.8 Limitation 19

3 Near-field antenna measurement system 20

3.1 Introduction of the system 20

3.2 Management component -- PC 21

3.3 Measuring equipment -- Vector Network Analyzer 22

3.4 Rectangular planar scanner 23

3.4.1 Scanner structure 23

3.4.2 A-BUS adapter and ST-143 dual step motor controller 25

3.5 Communication in system 27

3.5.1 Communication between PC and VNA -- GPIB 28

3.5.2 Communication between VNA and ST-143 dual motor controller 30

3.5.3 Communication between PC and Stepper motor controller 33

3.6 Operating and program results 35

4 Near-field to far-field transformation 41

4.1 Far-field dertermination from source distribution 41

4.2 Asymptotic evaluation of the aperture radiation field 44

4.3 FFT algorithm used for far-field 47

4.4 Algorithm application 49

4.5 One-dimensional near-field antenna measurement 51

4.6 Probe-correction 52

5 Validation of the system **54**

5.1 Description of antenna under test 54

5.1.1 L/C band microstrip antenna 54

5.1.2 Horn antenna 56

5.2 Test sample spacing 57

5.3 Test scan length and distance 57

5.4 Probe selection 59

5.5 test results 60

5.5.1 Test results for L/C band microstrip antenna 61

5.5.2 Test results for horn antenna 63

5.6 Comparison of the direct far-field 64

5.6.1 Anechoic chamber measurement system 65

5.6.2 Comparison of near-field and far-field results 66

5.7 Recommendation 70

6 Conclusion and Future Work **72**

6.1 Conclusion 72

6.2 Future Work 73

Reference **74**

Appendix I VNA calibration 77

Appendix II GBIB Commands - Calibration 81

List of Figures

2.1 Three field region 7

2.2 Antenna measurement configuration 10

2.3 Uniform sampling 18

3.1 Near-field antenna measurement system 21

3.2 PC management flowchart 22

3.3 Communication between PC and Analyzer 23

3.4 Near-field scanner 24

3.5 Schmatic of A-BUS Adapter 26

3.6 Schmatic of dual motor controller 27

3.7 Communication in system 28

3.8 Communication between PC and VNA 29

3.9 Probe operation 30

3.10 System communication setup 31

3.11 Trigger signal 32

3.12 PC management the motion of stepper motor controller 34

3.13 Near-field measurement system communication 35

3.14 Flowchart of near-field measurement process 36

4.1 Near-field measurement Ex, Ey, and step-length 48

4.2 Flowchart of process program 50

4.3 One-dimensional near-field measurement 51

5.1 L/C band microstrip antenna elements 55

5.2 Antenna under test: Microstrip antenna 56

5.3 Antenna under test: horn antenna 56

5.4 The angle of validity of the far-field 58

5.5 Probes used in tests 59

5.6 Comparison of different probes measurement results 60

5.7 Far-field radiation patterns of microstrip antenna 62

5.8 Far-field radiation patterns of horn antenna 64

5.9 Anechoic chamber measurement system 65

5.10 Comparison of L band microstrip antenna horiaontal radiation pattern 67

5.11 Comparison of C band microstrip antenna horizontal radiation pattern 68

5.12 Comparison of horn antenna horizontal radiation pattern 69

5.13 Near-field antenna measurement: Position 1 70

5.14 Near-field antenna measurement: Position 2 71

List of Tables

2.1 Definitions of Near- and Far-field Regions 7

3.1 Scanner structure factors 24

5.1 Device specifications 55

5.2 Near-field measurement characteristics (Microstrip antenna) 61

5.3 Near-field measurements of horn antenna 63

Table of Principal Symbols and Abbreviations

q	Charge coulomb
I	Current ampere
AUT	Antenna under test
E	Electric field volts/m
DFT	Discrete Fourier transform
FFT	Fast Fourier transform
B	Magnetic field webers/m^2
H	Magnetic intensity amps/m
NF	Near-field measurement
L	Length meter
D	Antenna width or diameter meter
d	Distance meter
θ_0	Maximum angel with accurate result
VNA	Vector Network Analyzer
GPIB	General Purpose Interface Bus
Z_0	Characteristic impedance of free space (377Ω)
R	Radiation Diameter meter
λ	Wavelength
PC	Personal Computer

∇x	Grid spacing along x-axis
∇y	Grid spacing along y-axis
z_t	Distance between AUT and probe
h	hour
PWS	Plane wave spectrum
m	meter
sec.	second
f	frequency
RF	Radio Frequency
TT&C	Telemetry, tracking, and command

Chapter 1

Introduction

1.1 Statement of the problem

The measurement of an antenna far-field radiation pattern is an important topic in the development and manufacture of sophisticated antennas. Techniques used for the measurement of antenna far-field radiation patterns can be classified into two general categories: direct and indirect [1].

The distribution of the radiated electromagnetic field from an antenna changes gradually with distance from the antenna. Distances from the antenna lie in basically two main regions: near-field and far-field regions.

The antenna's direct far-field radiation pattern measurement techniques are performed in the far-field region [2]. Such techniques are becoming less capable of determining the performance of advanced antennas. This is due to a variety of problems, including weather effects, multipath and antenna gravitational distortions, and security [2]. When antennas are very large or when the final stages of assembly occur at the installation site, the direct measurement of accurate far-field radiation patterns is extremely difficult and usually erroneous.

Indirect techniques, referred to as near-field techniques, are developed on the fact that the quality of a far-field or compact range can be determined by the near-field region measurements, and then these measurements can be converted by mathematical transformation to the equivalent far-field measurements. Near-field testing offers all of the advantages of indoor operations (i.e., all-weather, source, compact) plus information on the details of the aperture illumination that otherwise can only be inferred indirectly. Further, because the antenna under test does not need to be moved, large and fragile structures can be tested without adding stresses and associated deflections [3].

Use of near-field antenna measurements to determine far-field radiation patterns has become widely used in antenna testing since they allow for accurate measurements of antenna patterns in a very cost-effective and efficient manner, as well as a controlled environment. Although a commercial near-field/far-field measurement system has been developed, it is very expensive. The basic theme of this thesis is that a low cost near-field/far-field measurement system is designed, built, and validated in C-CORE, Memorial University of Newfoundland. All relevant software programs are developed for near-field/far-field transformations in a user friendly way.

1.2 Research Background

For more than 20 years, near-field/far-field measurement techniques have been formulated and applied to the measurement of antenna radiation and target scattering [4]. The theory, computer programs and experimental procedures have been successfully developed for the determination of complex radiation and scattering from measurements taken on planar, cylindrical, and spherical scanning surfaces in the near-field.

By definition, near-field measurements are done by sampling the field close to the antenna on discrete locations on a known appropriate imaging surface. From the measured phase and amplitude data in the near-field at the location, the far-field pattern can be computed in much the same fashion that theoretical patterns are computed from theoretical field distributions for aperture antennas. The transformation used in the computation depends on the shape of the imaging surface over which the measurements are taken with the scanning probe [3].

This imaging surface where scanning takes place can be either planar, cylindrical, or spherical. The basics of the processes are similar in the three methods. Planar scanning is more frequently used in near-field measurements than cylindrical and spherical scanning because most directive antennas have, on or near the antenna, an "aperture distribution" or "aperture illumination" of finite extent slightly larger than the projected area of the antenna [3].

Basic near-field techniques determine the equivalent far-field antenna performance through two basic steps:

(1) Measure the phase front of the antenna under test (AUT) using a microwave interferometer probe positioned by a robot.

(2) Sort the phase front into the actual directions of energy propagation using Fourier transform (FT) techniques. The result is an angular spectrum (antenna pattern). The angular spectrum in the near-field is the same as the angular spectrum in the far-field because electromagnetic energy in free-space travels in a straight line [3].

1.3 Scope of the work

In order to develop a near-field to far-field antenna measurement system, the following has been done:

(1) Build a near-field measurement system, which includes hardware and software parts. a) A planar scanner; b) A vector network analyzer; c) A PC and relevant software programs for communication and management.

(2) Perform near-field antenna measurement using the near-field antenna measurement system.

(3) Apply near-field to far-field antenna measurement transformation to get the far-field antenna radiation pattern.

(4) Validate the system by comparing the results with far-field radiation patterns which are directly measured inside C-CORE's anechoic chamber for a number of prototype antenna models.

(5) Study is performed to compare the size of scanning grid on accuracy of results.

(6) Linear scanning is presented.

(7) The system software is developed as a user friendly code for further use by technical personnel.

1.4 Organization of the thesis

This thesis is organized as follows: Chapter 2 briefly reviews the techniques of near-field/far-field antenna measurement where various algorithms are presented. Chapter 3 describes the development of the planar near-field antenna measurement system. Chapter 4 describes the algorithm of near-field/far-field antenna measurement transformation. In chapter 5, measurement results are presented and compared with direct far-field antenna

measurements as well as comparisons between linear and planar scanning techniques. A study of the scanning parameters is also presented. Chapter 6 concludes the thesis with a summary of results and suggestions for further research.

Chapter 2

Literature Review

2.1 Definition of near-field and far-field

The distribution of radiated electromagnetic field associated with an antenna changes gradually with distance from the antenna. Three regions, as a function of distance from the antenna, are of interest; reactive near-field, radiating near-field and far-field. The transitions between these regions are quite gradual and the boundaries are not distinct. There are many different definitions for near-field and far-field limitations [2, 3, 5, 6 - 11]. The definitions used in this thesis are given in Figure 2.1 and Table 2.1, where the following descriptions are used:

1. The region nearest to the antenna is the evanescent or reactive near-field region. The evanescent component of the electromagnetic energy decays very rapidly with distance. The evanescent region includes both nonpropagating (reactive) and propagating energy, and extends from any conductive surface for a distance of one sixth of the wavelength.

2. The second region is the radiating near-field or Fresnel region. It extends to $2D^2/\lambda$, where λ is the wavelength and D is the largest dimension of the antenna. The

average energy densities remain relatively constant at different distances from the antenna although there are localized energy fluctuations. In this thesis the near-field measurements are done for the radiating near-field region of the AUT.

3. The region farthest from the antenna is the far-field or Fraunhofer region. The relative angular distribution does not vary with distance in the far-field region. The power radiated from an antenna in the far-field region decays according to the inverse square law as a function of distance. The far-field region extends from $2D^2/\lambda$ to infinity.

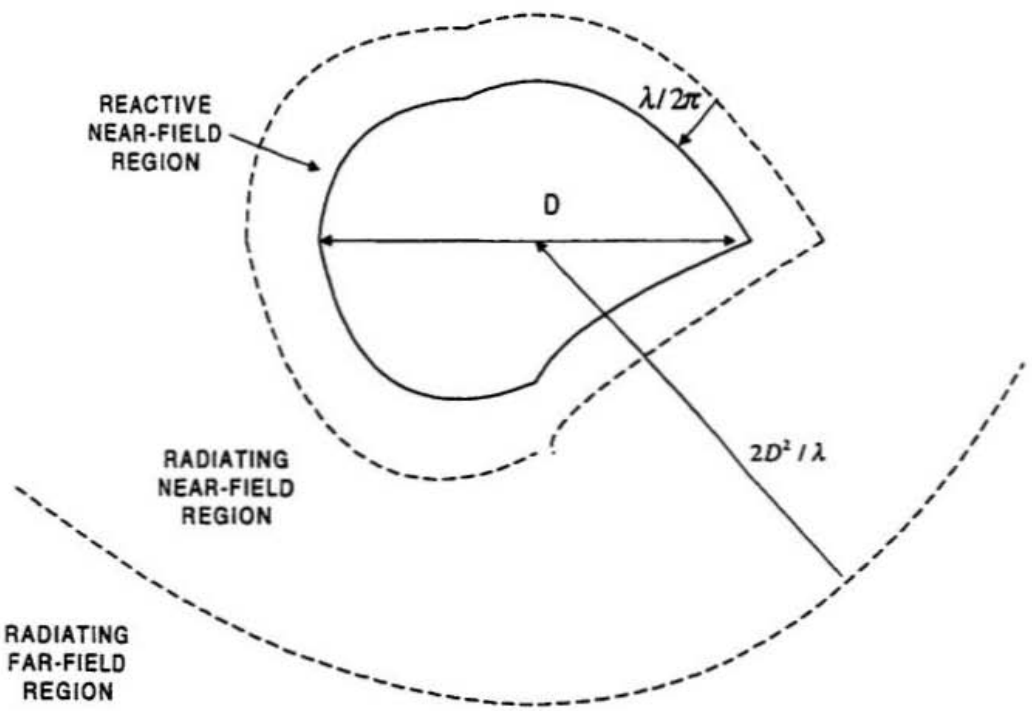

Figure 2.1 Three regions of electromagnetic fields produced by an antenna

Table 2.1 Definitions of Near- and Far-Field region [2, 8]

	reactive near-field	radiating near-field	far-field
Near limit	0	$\lambda/2\pi$	$2D^2/\lambda$
Far limit	$\lambda/2\pi$	$2D^2/\lambda$	∞
Power decay	R^{-n}	1	R^{-2}
E and H orthogonal	no	yes	yes
Z_0	no	yes	yes

In this table, Z_0 is the characteristic impedance of free space, and

$$Z_0 = 377\Omega$$

2.2 Near-field measurement concepts

There are two general categories of measurement of antenna far-field pattern techniques: direct or indirect. In the direct techniques, the far-field is the measured quantity; whereas in the indirect techniques, referred to as the near-field techniques, the far-field is only a byproduct which is constructed from measured near-fields in the vicinity of the antenna [1].

The antenna radiates into free space as a linear system with the single-frequency time dependence of *exp(-iwt)*. The far-field region which extends to infinity, is that region of space where the radial dependence of electric and magnetic fields varies approximately as *exp(ikr)/r* [5]. The inner radius of the far-field can be estimated from the general free-space integral for the vector potential and is usually set at $2D^2/\lambda$ for nonsuper-reactive

antennas. The free-space region from the surface of the antenna to the far-field is referred to as the near-field region. It is divided into two subregions, the reactive and radiating near-field. The reactive near-field region is commonly taken to extend about $\lambda/2\pi$ from the surface of the antenna, although experience with near-field measurements indicates that a distance of a wavelength (λ) or so would form a more reasonable outer boundary to the reactive near-field. Beyond a distance of about a wavelength from nonsuperreactive antennas, the electric and magnetic fields tend to propagate predominantly in phase, but of course, do not exhibit *exp(ikr)/r* dependence until the far-field is reached. This propagating region between the reactive near-field and the far-field is called the radiating near-field.

Evanescent energy is coupled to the near-field probe capacitively or inductively, but not by free-space propagation. Because of this, the $\boldsymbol{E}$ and $\boldsymbol{H}$ fields are not orthogonal or related by the impedance of free space (377Ω) [2]. The evanescent energy decays very rapidly with distance because the evanescent energy is nonpropagating but reactively, capacitively or inductively, coupled. The evanescent energy normally has completely decayed at a distance of several wavelengths from a conducting surface. Near-field measurements are generally made outside of the evanescent region. Otherwise, higher sampling densities and separate $\boldsymbol{E}$ and $\boldsymbol{H}$ field measurements are required.

Near-field measurements are usually made in one of three coordinate systems: planar, spherical, cylindrical according to different scanning systems. The antenna far-field radiation pattern measurement techniques are outlined in Figure 2.2. Assuming the test antenna to be transmitting, the near-field can be broken down roughly into a reactive region within $\lambda/2\pi$ of the surface, and the radiating region outside of this, eventually merging into a far-field region. Within the reactive region the electric and magnetic fields are not in phase and do not represent signals that will appear in the real space portion of

the antenna pattern. A probe antenna is placed in the radiative near-field region and the amplitude and phase of the received signal recorded. Probe antennas are small enough to pick up energy over wide angles while causing minimal disturbance to the field being measured. The probe is moved over the planar, cylindrical, or spherical surface in steps of less than half a wavelength, and the data is stored. Each data point is the combined signal from a region of the antenna determined by the probe pattern. In this case, probe correction has been developed. Using near-field/far-field transformation techniques, the angular space of the far-field pattern is deduced from the data set $\boldsymbol{E}$ in the aperture space at the probe scan plane [3].

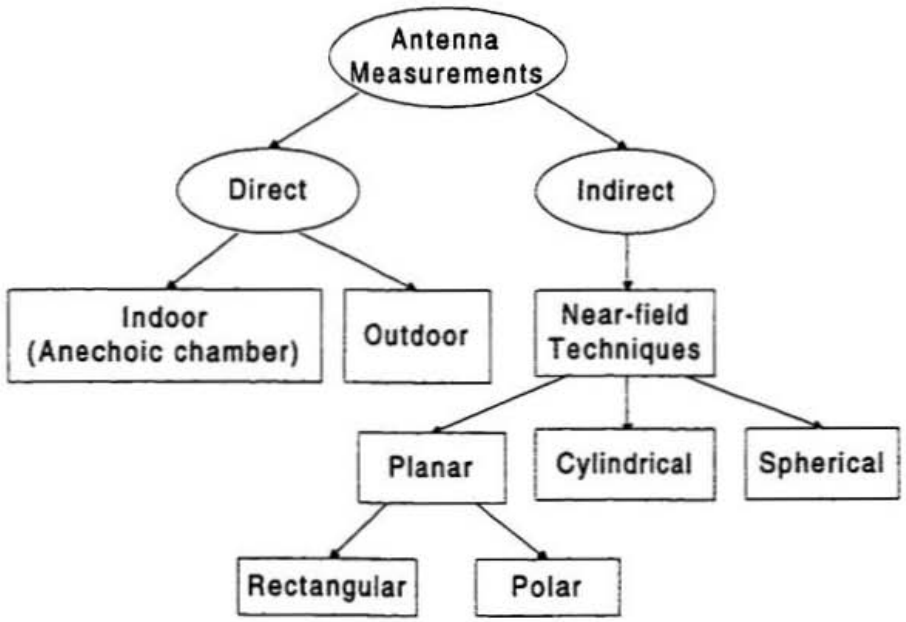

Figure 2.2 Antenna measurement configuration

The planar scan surface generally is preferred for high-gain spacecraft antennas, and just needs simple probe correction and has better zero gravity simulation. The spherical scan is used for low-gain antennas and antenna feed elements because the energy is

captured at large angles from the AUT boresight axis. Cylindrical surfaces are often used with television broadcast antennas and certain spacecraft TT&C omni antennas [2].

2.3 Advantage of near-field measurement

When direct antenna measurement is performed outdoors, it may be affected by weather conditions, multipath, etc.; when it is performed indoors, it needs to be measured inside an expensive big size anechoic chamber. Because of this, near-field measurement techniques are widely used today. Near-field techniques a) can give absolute measurements including mismatch corrections, b) need not involve approximations (in the extrapolation methods) other than truncation of the infinite set of exact solutions used in expressing the field, and c) apply to nonlinear transmitting transducers and nonreciprocal transducers (for example, arrays with ferrite phase shifters or isolators), whether transmitting, receiving, or scattering [12].

Additionally, from the technical point of view, some of the advantages of near-field measurement techniques over direct far-field pattern measurements include

(1) Near-field measurements are time and cost effective, and the accuracy of the computed patterns is comparable to that for the far-field range.

(2) The near-field range provides a controlled environment and all-weather capability.

(3) For large antenna systems, far-field range size limitations, transportation and mounting problems, and the requirement for large-scale positioners are eliminated.

The main advantage of near-field over direct far-field pattern measurements is cost. It is much cheaper to build a scanner than building an anechoic chamber on acquired land for antenna measurements.

2.4 Near-field antenna measurement criteria

2.4.1 Grid spacing criteria

The objectives of these sections are to establish a sample spacing criterion for near-field measurements made on a plane surface near the antenna under test (AUT), and to develop a near-field data minimization technique for reducing the computational effort required to calculate a given portion of the far-field radiation pattern [13, 14].

When the probe is operating on a polar-planar scanning plane, the probe increment between rings is usually taken at approximately 0.5 wavelength [1]. It follows from the two-dimensional Nyquist sampling theorem that, for the wavenumber limited spectrum, the electric field can be reconstructed for all points on the plane $z=0$ from a knowledge of its values at the rectangular lattice of points separated by the grid spacing of an upper limit of $\lambda/2$ [14].

2.4.2 Distance criteria

The required sample spacing depends on the distance from the antenna to the measurement plane and on the extent to which evanescent waves could be neglected [14]. Also, the sampling criteria assumes that the separation distance between the probe and test antennas is large enough to prevent significant coupling of their reactive fields [5]. Some researchers suggest that when the step-length is half a wavelength, the plane should be put in front of a source (AUT) of 10 wavelengths. Accordingly, the resulting fields are quite independent of the sample spacing as long as they are half a wavelength or less. The general practice in minimizing antenna coupling is to select the distance, between the antenna and the grid plane, large enough so that the VSWR of the probe, when operating as a transmitter, is insensitive to the presence of the antenna under test. Since probes with medium gains, such as 8-15dB, have been the preferred choice, the distance of 6-12 wavelengths was selected in most studies. The popularly used medium-gain probes (about 8-20 dB gain) were believed to have the advantage of filtering out range clutter [13]. A distance of 2-10 wavelengths is also suggested and used in near-field antenna measurements [17]. In our system, the distance between AUT and the plane is about 1-10 wavelengths.

2.5 Algorithms used

In order to construct far-field radiation patterns of antennas from the electric near-field measurements, uniform sampling techniques and a Jacobi-Bessel algorithm have been widely used in the past few years [15]. There are diverse methods for calculation of far-field patterns depending on the ways in which data are acquired. They can be classified as:

(1) the uniform sampling in a rectangular coordinate system;

(2) the uniform or pseudo-uniform sampling in a polar coordinate system;

(3) the non-uniform sampling in a rectangular or polar coordinate system.

A Jacobi-Bessel algorithm has been used to calculate the far-field patterns in all the above classes of measurements [15]. Recently an FFT algorithm has been proposed instead of the Jacobi-Bessel algorithm. Compared with the Jacobi-Bessel algorithm, the FFT algorithm considerably reduces the time of calculation [1, 15].

In near-field measurement, the probe moves in two orthogonal linear directions. The results are distributed in a rectangular coordinate system and the uniform sampling technique and FFT algorithm can be applied.

Far-field patterns may be calculated by using the FFT, given a set of near-field data which have values on a rectangular coordinate system. It can be shown by application of the Lorentz reciprocal theorem that the output voltage of the near-field measurement probe is proportional to the antenna electric and magnetic fields E_a and H_a. It can also be shown that the relation between the motion of the probe in the measurement plane and the antenna is a convolutional expression of the probe fields and the antenna fields E_a and H_a [2]. For polar scanning, the four-point Lagrange interpolation algorithm was first used in order to use FFT to get far-field patterns [16].

2.6 Validation

Validating the accuracy of any antenna measurement facility is difficult as there exists no standard antenna with an associated standard antenna pattern which can be measured to verify performance and assess accuracy. The two tangential field components of a

planar, cylindrical, or spherical surface enclosing the AUT and separated from the antenna by a distance of 2-10 wavelengths are measured in amplitude and phase at preselected sampling points over a prescribed portion of the enclosing surface in near-field measurement systems. The accuracy of a far-field pattern depends on the near-field measurement and the related measurement error through a modal transform [17].

The near-field measurement and associated measurement error through a modal transform determines the accuracy of the far-field pattern. Thus, approximate correction factors are needed in order to account for the finite size and near-field distance of the measurement probe [5, 18]. The major components of a near-field measurement system which affect measurement accuracy can include hardware and software parts; they are:

(1) finite scan area

(2) distance between the probe plane and the AUT

(3) receiver nonlinearities in measuring the near-field amplitude

(4) sometimes multiple reflection

(5) the chamber, the computer and associated software [5, 17].

(7) the near electric field pattern of the probe

(8) reflection from scanner support

The position drive system most commonly used is a dc variable-speed electric motor coupled to the moving members by a chain or lead screw. Desirable characteristics of the drive system are smooth operation and constant velocity with minimum vibration over a wide velocity range [4].

It is recommended that the amplitude and phase indications of the receiver are measured over a time interval of 8 h. The measurements begin after a 24-h warm-up of both the receiver and the RF source. The amplitude and phase measurements are repeated

at +3°C and -3°C from the nominal temperature value [17]. In our system, the measurements begin after about 1-h warm-up.

Several criteria were considered in the development of the procedure to be used in measuring the antenna far-field radiation pattern. These included repeatability of pattern data, repeatability of system test power levels, accuracy of measurement, capability of monitoring the signal levels continuously, and dynamic range to make gain measurements between two antennas of significantly different gains [1].

Several aspects of the measurement technique must be considered. Both receiver and amplifier gain (which are independently adjustable) must remain constant during the test, which may last as long as several days. In order to relate the reference levels of a particular configuration to the antenna's radiated power, the receiver and computer voltage levels are recorded while the probe is positioned at one spot on the near-field of the antenna. This spot is generally chosen to be approximately the point of highest power, and is referred to as the "hot spot". In order to obtain the most dynamic range of the receiver/computer, the probe is placed at this location and the receiver amplitude gain is set below saturation, still in its linear region [1].

2.7 Planar scanning of near-field measurement

The development of near-field antenna measurement techniques can be divided into four periods: the early experimental period with no probe correction (1950-1960), the period of the first probe-corrected theories (1961-1975), the period in which the first theories were put into practice (1965-1975), and the period of technology transfer (1975-1984) in which 35 or more near-field scanners were built throughout the world [5, 19].

Modern planar scanning techniques in near-field measurement of antennas and scatters are based on the plane-wave spectrum (PWS). Planar scanning is more frequently used in near-field measurements than cylindrical and spherical scanning because most directive antennas have, on or near the antenna, an "aperture distribution" or "aperture illumination" of finite extent slightly larger than the projected area of the antenna [13]. Aperture antennas are most common at microwave frequencies, and they may take the form of a waveguide or a horn whose aperture may be square, rectangular, circular, elliptical, or any other configuration [20]. For high-gain antennas, the planar configuration is used most frequently [1].

2.7.1 Near-field sampling

In the planar near-field measurement technique, data are acquired on a plane which is finite in extent but which intercepts the major portion of the radiating field. These data are then used to calculate the far-field quantities of the antenna under test. The calculation of the various quantities depends on the manner in which the data are acquired. Two different near-field sampling coordinate systems are used to complete the planar near-field measurements. One is measured in a rectangular coordinate system, and the other one is in a polar coordinate system. Generally, three kinds of sampling in planar near-field measurements are applied:

(1) the uniform sampling in a rectangular coordinate system;

(2) the uniform or pseudo-uniform sampling in a polar coordinate system;

(3) the non-uniform sampling in a rectangular or polar coordinate system.

Figure 2.3 shows uniform sampling in a rectangular or a polar coordinate system.

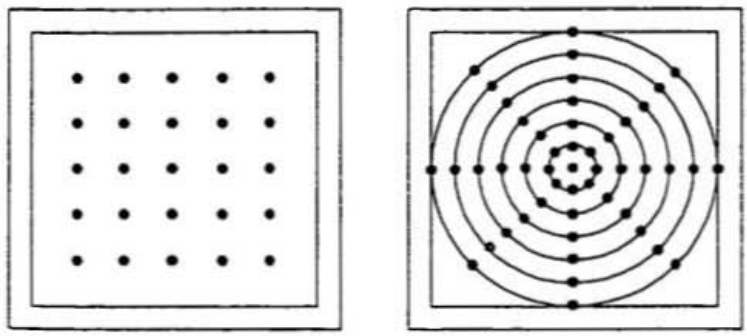

Figure 2.3 Uniform sampling

Accordingly, different mathematical transformations are used for different kinds of sampling coordinate systems. Considering the computing and application convenience, near-field uniform sampling in a rectangular coordinate system is preferred.

The first step in a near-field measurement is to sample the fields at the near-field s' plane. The antenna near-field problem in rectangular coordinates is particularly suitable for the FFT technique because their near-field and PWS are both of finite extent; that is, they are "almost space-limited" and "almost band-limited", respectively. As a result, sampling and filtering techniques dealing with general band- and space-limited signals have been found overly restrictive for the antenna problem [13].

2.7.2 Rectangular-planar near-field measurement

In the planar near-field measurement technique, the data acquisition scheme required the probe to move in two orthogonal linear directions in rectangular coordinate systems. This provides data which are in a rectangular coordinate system and thus the application of Fourier transform methods, by using the fast Fourier transform (FFT), becomes the

obvious data reduction technique [16]. Near-field data are acquired on a plane which is finite in extent but which intercepts the major portion of the radiation field. The far-field pattern is calculated from the measured near-field. When it is assumed that multiple interactions between the probe and the test antenna are negligible, probe-corrected planar near-field formulas can be used [18].

2.8 Limitations

1. Planar, cylindrical, and spherical near-field scanning can be formulated to include all the multiple interactions between the probe and test antenna [5].
2. Another limitation (besides the neglect of multiple reflections) within the basic theory of planar near-field scanning limits the application of planar scanning to directive antennas [5].
3. Because of the size of the near-field measurement scanner, the far-field antenna radiation pattern we get from near-field measurement cannot be 0~360° or -180°~180° as the horizontal radiation pattern we measured by direct antenna measurement inside the anechoic chamber.

Chapter 3

Planar Near-Field Antenna Measurement System

3.1 Introduction of the system

A typical near-field measurement system can be conveniently described in terms of three subsystems: (1) computer (2) RF source and receiver (3) mechanical scanner and probe positioner. A great deal of variety is possible for each of these subsystems [20].

The developed planar near-field measurement system which is built in C-CORE, Memorial University of Newfoundland, is mainly made of a Personal Computer (PC) 286, a $1.5m \times 1.5m$ planar scanner, and a Wiltron model 360 Vector Network analyzer (VNA). The PC and the VNA already belong to C-CORE's RF anechoic chamber measurement system. The cost of the newly planar scanner including relevant control part is less than $2000. The system structure is presented in Figure 3.1:

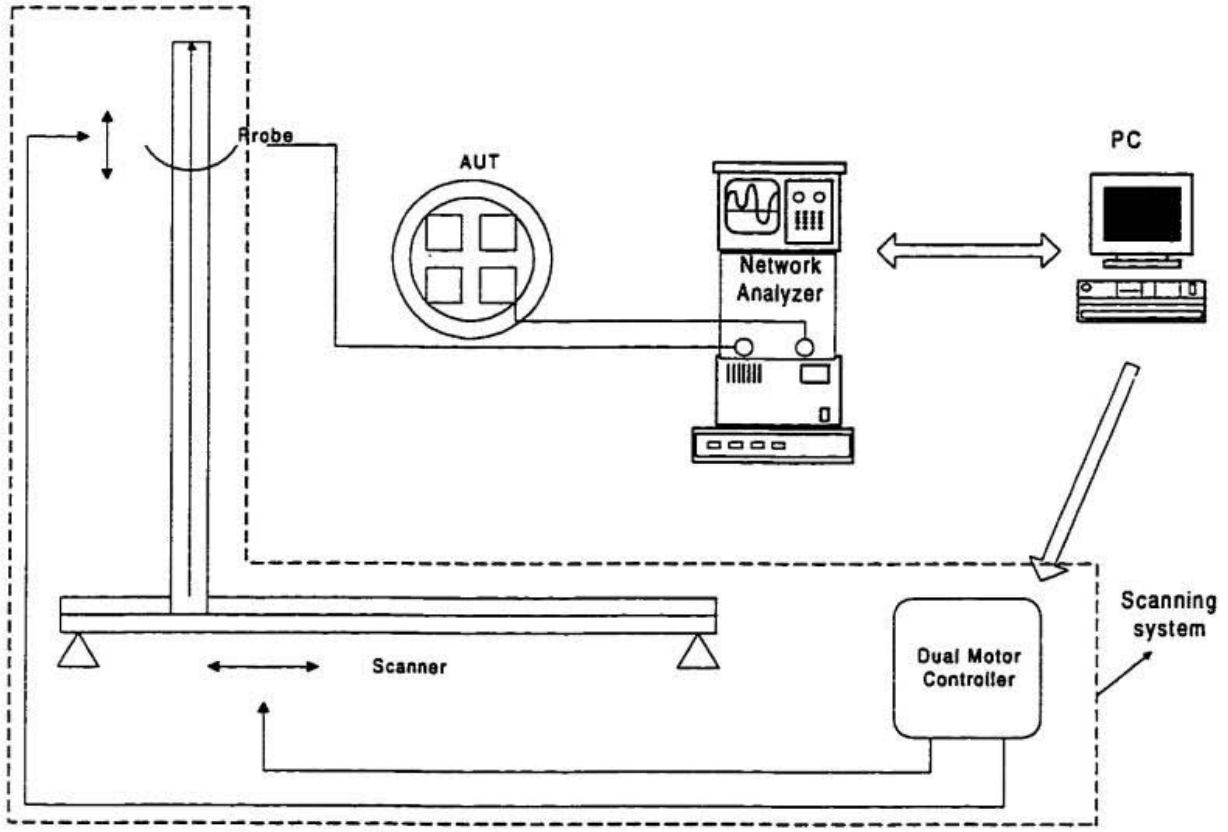

Figure 3.1 Near-field antenna measurement system

The probe on the planar scanner is driven by the dual motor controller, and moves in horizontal and vertical directions. At certain positions, the probe will measure the magnitude and phase of the near electric field radiated by the AUT which is kept at a certain distance from the scanning plane, and shows on the VNA. After several measurements, the VNA will pass these data magnitude and phase to PC storage for further processing..

3.2 Management component--PC

Because of the large amounts of data involved, computer control of the measurement system is essential. The PC in the near-field antenna measurement system performs the management duty,

controls the motion of the probe, collection of the data from VNA, and also the management of the communication between VNA and PC. The management package is written in Quickbasic embedded Assembly languages. The management is performed in real time as shown in Figure 3.2.

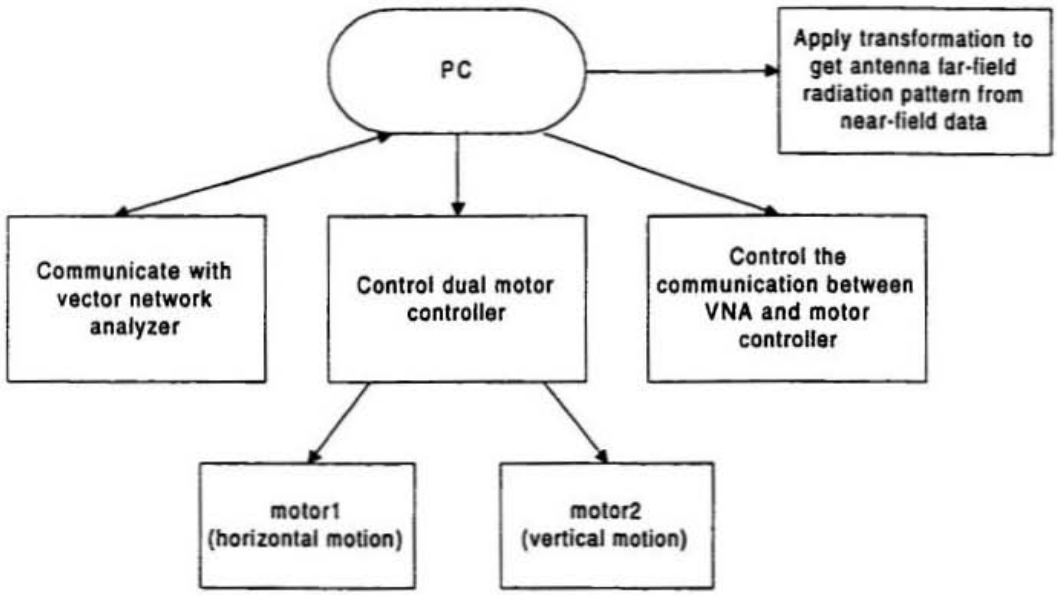

Figure 3.2 PC management flowchart

3.3 Measuring equipment -- Vector Network Analyzer

A two-port Wiltron model 360 VNA, already part of C-CORE's RF anechoic chamber measurement system, is used in the near-field antenna measurement system to measure the radiation pattern of AUT. It is made of a front panel, a screen, a generator, and a source, has a frequency range of *40MHz - 40GHz*, and frequency resolution of *100KHz*.

Before starting a measurement, the VNA calibration needs to be done. For near-field antenna measurement, full-term calibration is preferred, which includes reflection and frequency response calibration.

When the calibration is performed on the front panel of the VNA, the measurement option menus are listed in Appendix I [21]; when the calibration is performed by the PC through GPIB, the commands are listed in Appendix II [22].

The communication between the PC and VNA is detailed in Figure 3.3.

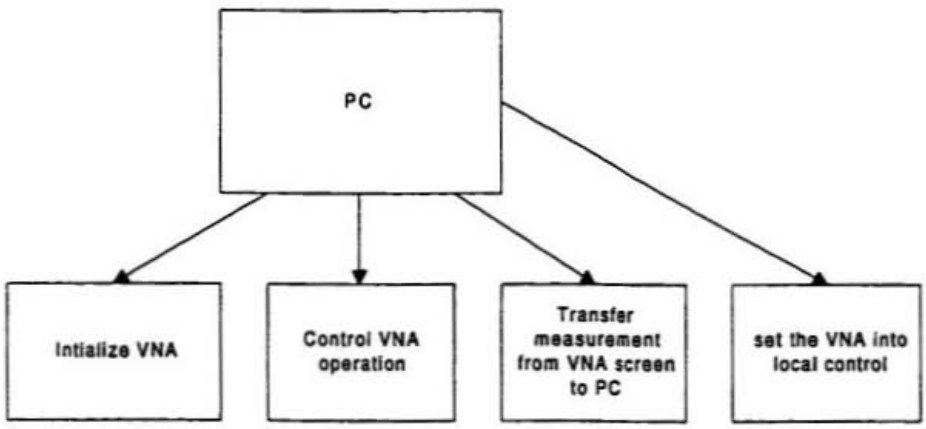

Figure 3.3 Communication between PC and Analyzer

3.4 Rectangular Planar Scanner

3.4.1 System structure

The mechanical scanner (or probe positioner) consists of the supports, guides, and drive motors to move the measuring probe from a given x-y coordinate in a plane to certain point until a

reading is taken. The span of the scanning plane can reach 1.5 meters in both the vertical and horizontal directions which can follow in a specific pattern as shown in Figure 3.4 [23].

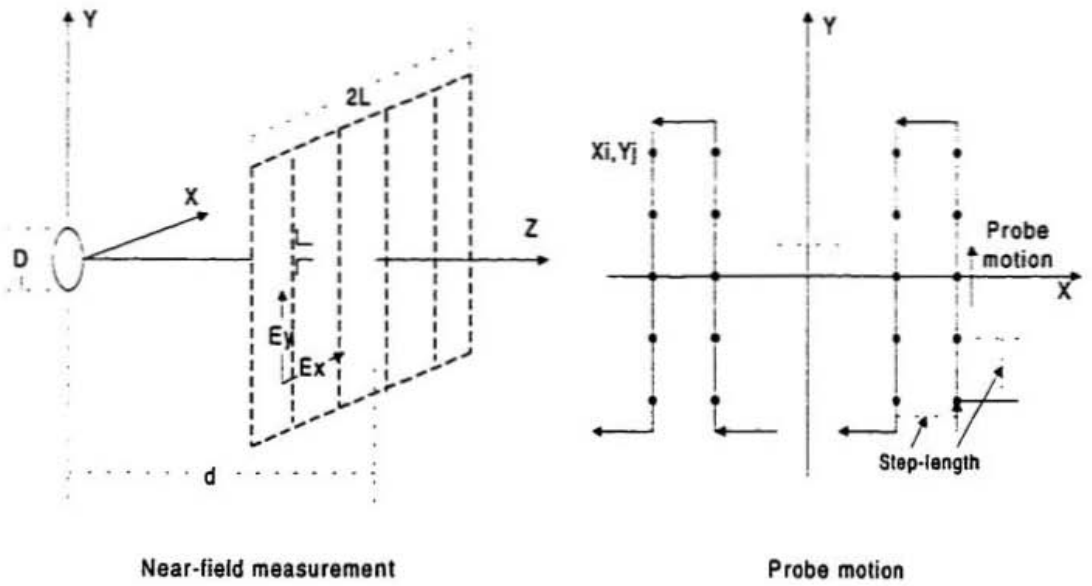

Figure 3.4 Near-field scanner

The mechanical structure of the scanner consists of a horizontal and a vertical axis each with its own drive mechanism such that either axis can be driven independent of the other. The advantage of the structure is shown in the following table 3.1 [23]:

Table 3.1 Scanner structure factors

Size	Carriage	Drive screw	Step
1.5m×1.5m	5 pounds	1/4"×20 threads/inch	200 step/sec.

The electrical design consists of an electronic interface with a PC. A computer driven pair of stepper motors position the test probe at predetermined points in a grid of maximum planar size of 1.5m × 1.5m. This design enables the planar scanner to be set up inside C-CORE's anechoic chamber which is 4m × 2.5m × 2.5m. Control from the computer is capable of stopping the probe at determined intervals and allows time for a measurement to be taken from the VNA.

According to the design, as the motors are incremented, the number of steps moved are used to calculate a vertical or horizontal linear displacement.

$$Displacement(meters) = number\ of\ steps \times 7.5\ degrees / 20 turns/inch \times 0.0254$$

Using this equation, one can calculate relative motor running turns to determine the probe position.

3.4.2 A-BUS Adapter and ST-143 dual step motor controller

An AR-133 card, A-BUS adapter which can be used for the IBM PC/XT/AT and all compatibles, is connected with the step motor controller. A-BUS adapter which can be inserted into the PC, converts the signals available on the PC to the universal A-BUS standard. This insures that any current or future A-BUS card will work with the system. It has four essential design goals: (1) Reliability: quality components, uncompromised design; (2) Low cost: savings are achieved by clear design and efficient bus structure; (3) Simplicity and Expandability; (4) Universality.

The complete A-BUS system that we used consists of a driver circuit, AR-133, which is an A-BUS Adapter and located on the 16-bit bus internal to the computer. The schematic of AR-133, the A-BUS adapter, is shown in Figure 3.5.

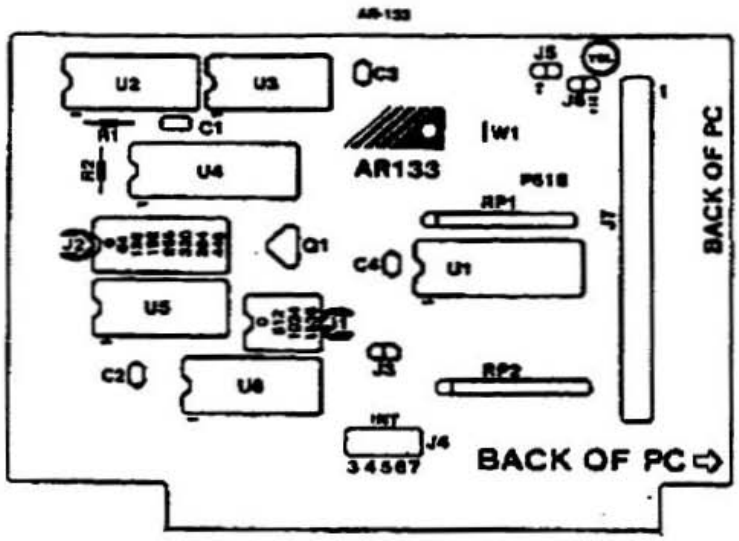

Figure 3.5 The schematic of AR-133

The external board, ST-143, is the amplifying circuit for the internal board. ST-143 is powered by a 700ma 9-volt adapter. The internal board accepts signals from the computer and processes a sequence of pulses which are required to drive the stepper motors. These signals are then sent to the external board where they are amplified and sent to the stepper motors. The schematic of ST-143 dual motor controller is shown in Figure 3.6.

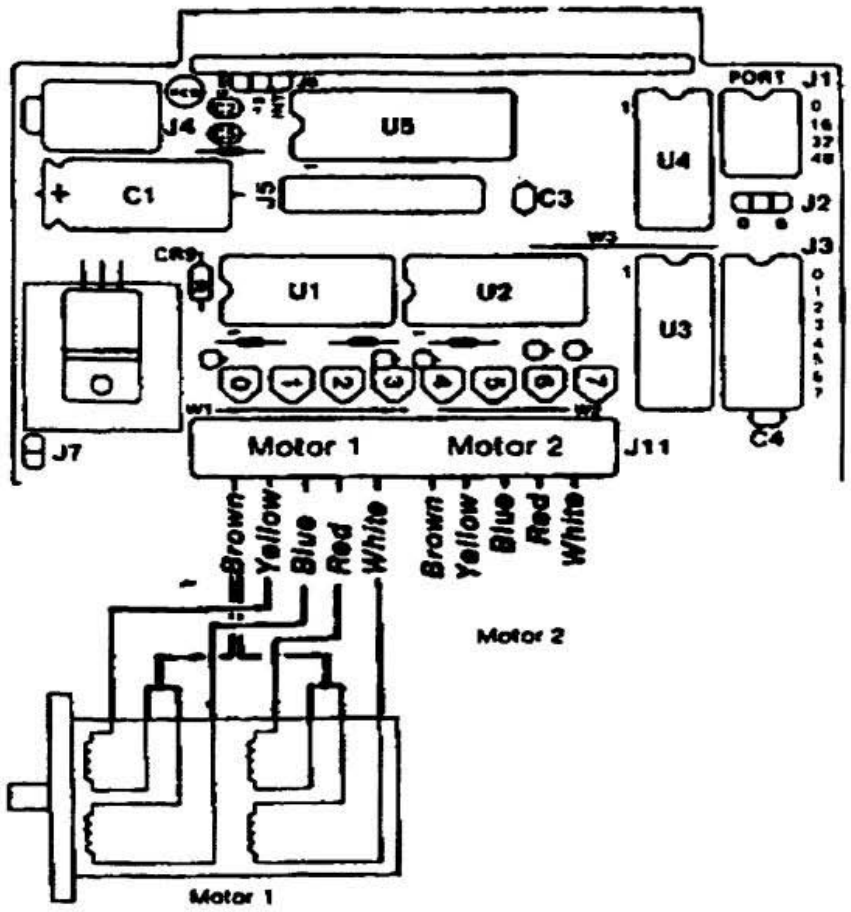

Figure 3.6 Schematic of dual motor controller

3.5 System Communication

In order to record the near-field antenna measurement data picked up by the probe, communication is built between the dual stepper motor controller, the PC, and the VNA. Different communication components are used for different proposes. The basic system communication structure is shown in Figure 3.7.

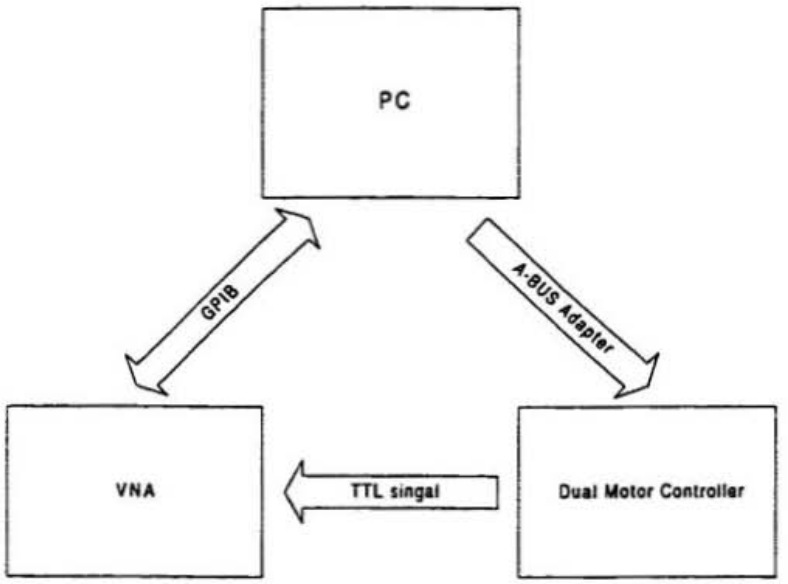

Figure 3.7 Basic communication in system

Running the control program, the probe will be driven by the dual stepper motor controller and move along vertical or horizontal direction. After the probe reaches the predetermined position, a trigger signal is given to the VNA by ST-143, the magnitude and phase on the position are recorded. After recording one line, the motor will drive the probe vertical support on the other direction at one step-length, also the VNA will pass the data, which includes amplitude and phase, to the PC. The PC will store the data along one line into a file with a name supplied by the user. This process will be repeated until one square planar sampling is finished. Several data files will be obtained after the near-field measurements are finished.

3.5.1 Communication between PC and VNA--GPIB

The communication between the PC and the VNA is through General Purpose Interface Bus (GPIB), an IEEE-488 interface, whose high data transfer rate is up to 1 megabyte/sec. The work

is done by a program written in Quickbasic embedded Assembly. The high data transfer rate satisfies the real time control demand. The flowchart is shown in Figure 3.8.

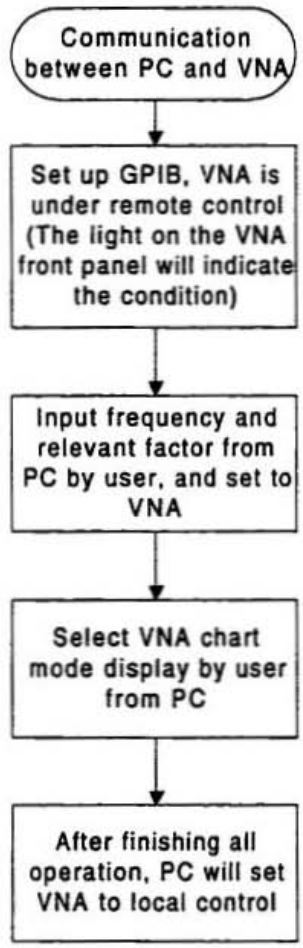

Figure 3.8 Communication between PC and VNA

There are three VNA chart modes available: a) Polar Format; b) Log Magnitude and Phase; c) both Polar and Rectangular. In planar near-field measurements, we use magnitude and phase. During the measurement, the VNA is not permitted to input data from the front panel until 'clear' is operated first. After finishing near-field measurements, the VNA will be returned to local control. The user can input data and operate on the front panel of the VNA.

3.5.2 Communication between VNA and ST-143 dual motor controller

As described before, when the probe reaches a certain position as shown in Figure 3.9, a trigger signal is demanded to activate the VNA. Then, the VNA measures the magnitude and phase of the AUT. Generally, the probe motion on the screen is discontinuous, it only picks up the magnitude and phase at the black dot points. Because the centered points should always be measured, the number of the measurement points should be odd.

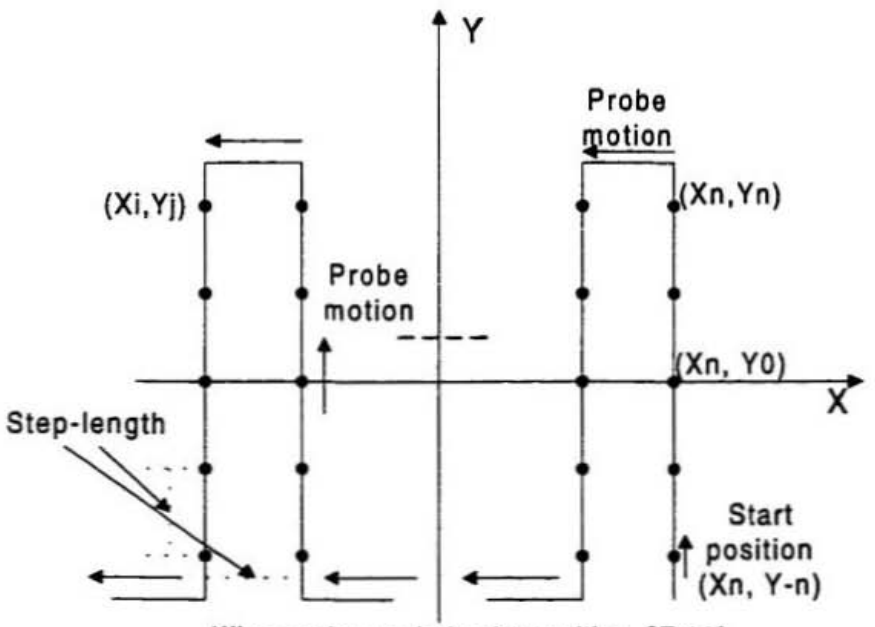

Figure 3.9 Probe operation

After setting up the system, the key task is to trigger the VNA360 which is shown in Figure 3.10. The magnitude and phase at certain locations shown as Figure 3.5.2 should be measured and recorded by the VNA360 in real-time. A trigger signal should be sent to the VNA whenever the probe moves a step-length, and it should be easy for the user to change the step-length by input from PC. The signal can be a separate signal and must give a trigger signal whenever demanded -- it must trigger the VNA360 when the probe is at certain positions. In order to get the trigger signal, several tests are needed.

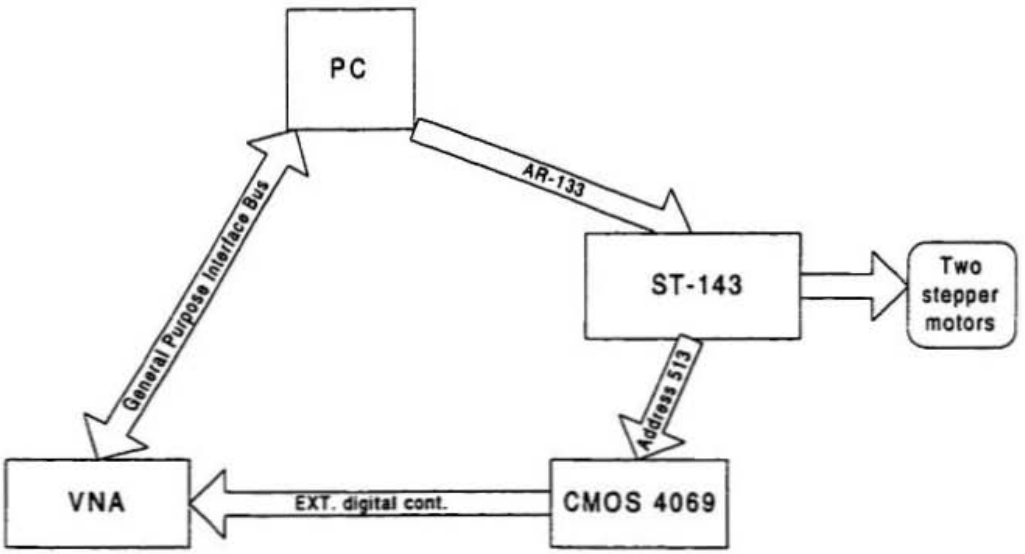

Figure 3.10 System communication setup

As the VNA is already in C-CORE's anechoic chamber measurement system, a scope is used to check the trigger signal (output) given by a NF90 series stepping motor controller, a VELMEX Inc. product, which is used to drive one motor to get the H-plane inside the anechoic chamber measurement system, and connect with VNA360. It is active high and the signal level is TTL.

In order to obtain the trigger signal for the VNA, we have tried several methods. First, get the signal from the out port of the A-BUS adapter, but signal level is different. Then signal for driving the motor has been tried. Its frequency does not match the need of the trigger signal.

After that, signal from RS-232 (serial port of PC) has also been tested, it is not a normal TTL. Finally, the trigger signal is obtained from ST-143 card I/O selection and then through CMOS 4069 (invert gate) to get the trigger signal as shown in Figure 3.11.

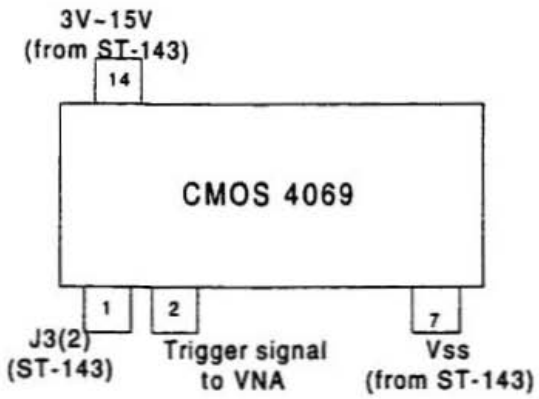

Figure 3.11 Trigger signal

The ST-143 card address is 512. Before moving the probe on the planar screen, the PC must select the right address to drive the motor. Its signal level is within TTL. Now, in order to give a trigger signal, another I/O address, not address 512, is selected. Because it is active low, an CMOS 4069 (invert gate) is used to get a reverse signal, then connected with the VNA360 EXT. Digital Control port. The VNA360 measures and records the data by the function which is written in my program.

The trigger signal and Vss are connected with the EXT. DIGITAL CONT. of the VNA. The function is finished by the following commands:

```
out 513, 1
for t=1 to 400: next t
```

where the last command is used for a piece of delay. When the VNA receives the trigger signal, the magnitude and phase picked up by the probe at certain locations are recorded on the screen of

the VNA. The motion is repeated until one vertical line measurement has been finished. Then the magnitude and phase measured are passed to the PC and saved as a data file.

3.5.3 Communication between PC and Stepper motor controller

As described before, the PC controls the function of ST-143, a stepper motor controller, through AR-133, an A-BUS adapter.

In the system, the A-BUS adapter, AR-133, is plugged into the computer, and connected with the A-BUS card, ST-143. The PC controls the motion of the stepper motor controller by software program. The program for driving the probe and giving the trigger signal to VNA is written in Quickbasic language, and is stored in the PC. The user just needs to interface with the PC. The flowchart of PC management of the motion of the dual stepper motor controller is shown in Figure 3.12.

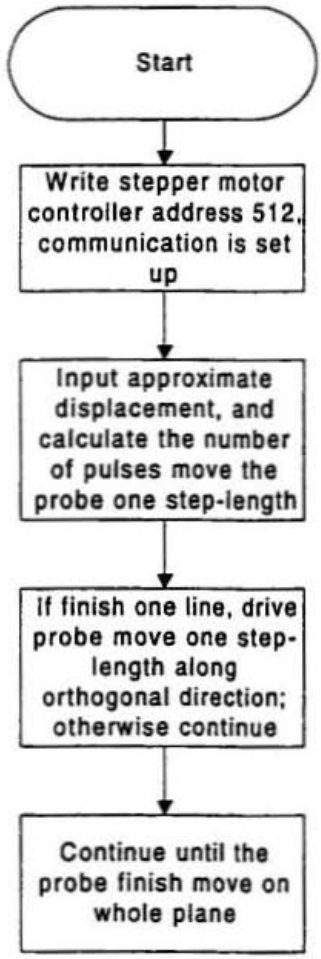

Figure 3.12 PC management of the stepper motor controller

After the communications between the PC and the VNA, the PC and the stepper motor controller, and the VNA and the stepper motor controller have been set up, the communication in the whole near-field measurement system is shown in Figure 3.13.

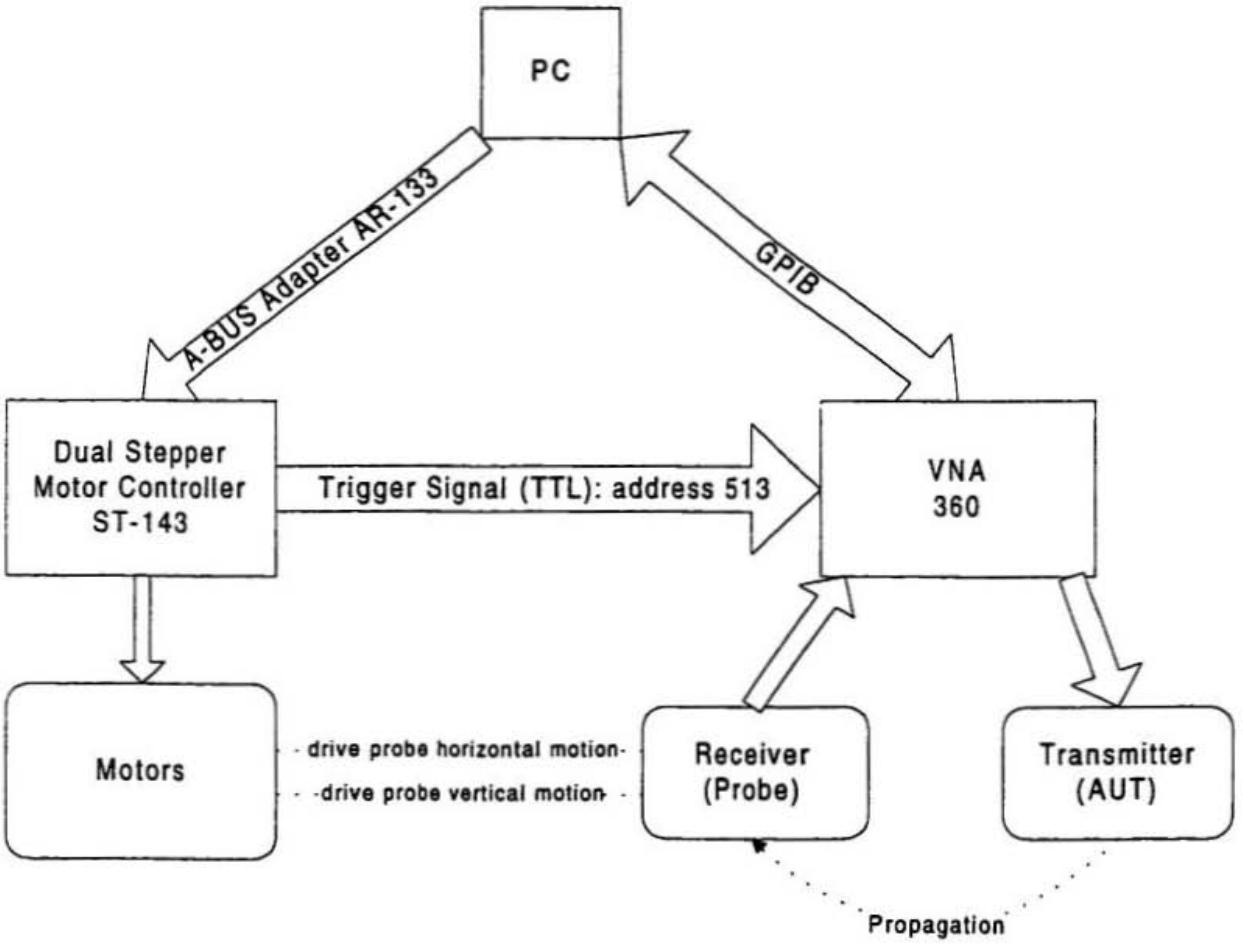

Figure 3.13 Near-field measurement system communication

3.6 Operating and Program results

In a near-field antenna measurement system, the PC controls the motion of the probe, the VNA, and the communication in the system. Since it performs a real-time control, the program is written in such a way that the functions are performed in separate time series. Quickbasic language is preferred, because it is simple, runs fast and available on most PC. The assembly language is embedded since it makes the running speeds up. The program has been created as an

executable file. User just need to type in the name N_F to run the program. Before running the program, the probe is put to be in the center of the scanning plane, and face the AUT. The location of the probe can be controlled by the program named move.bas, whose executable file is move. The operation flowchart and the operating steps are given in Figure 3.14.

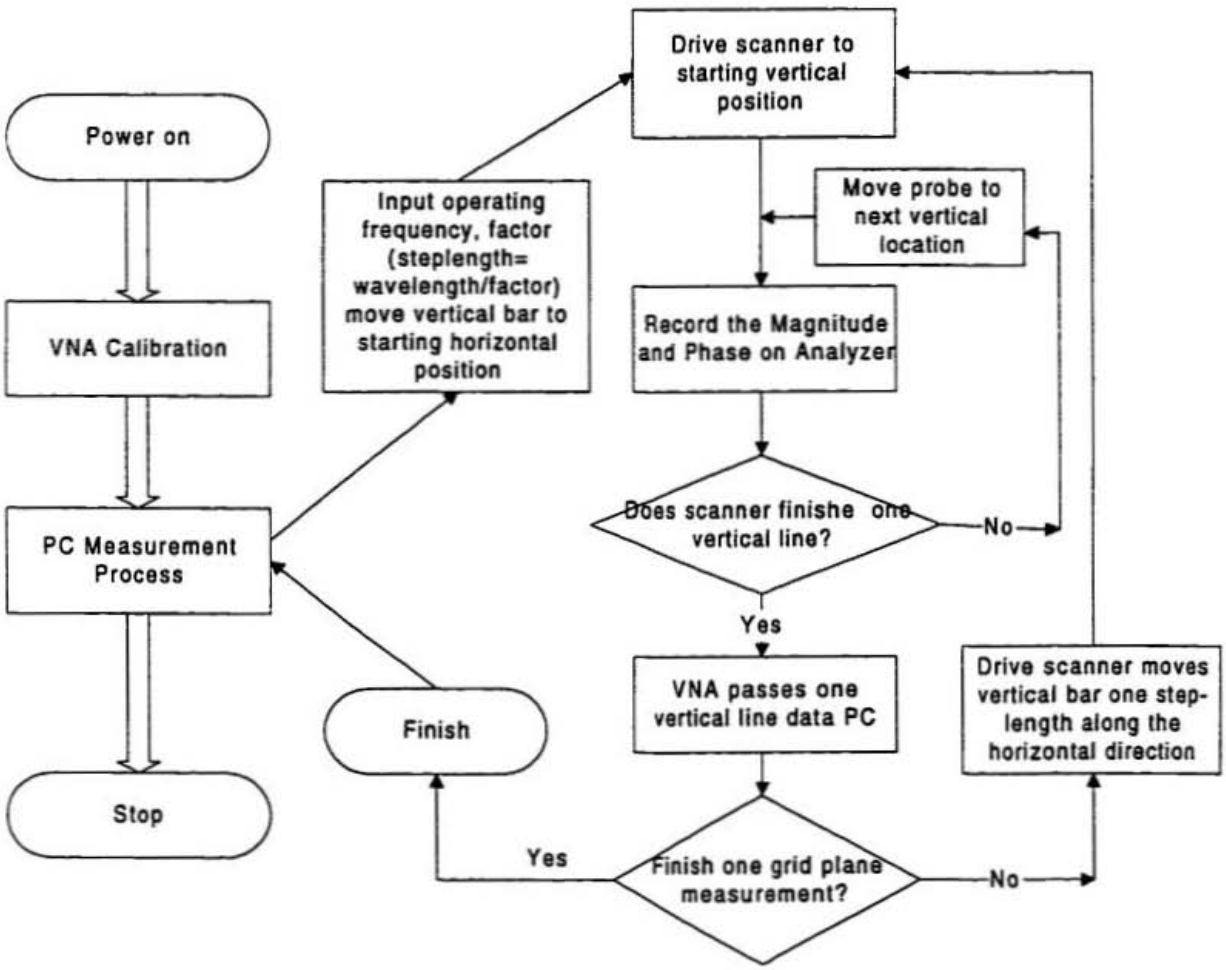

Figure 3.14 Flowchart of PC management

Before running the operating program, the operator should check the data files "di_x" and "di_y" which are direction files, and indicate whether the probe moves in a left/right and up/down direction according to the scanner condition. Then in running the controlling program, the following reminders will be given:

(1) After input the program name: N_F, the following will appear on the screen:

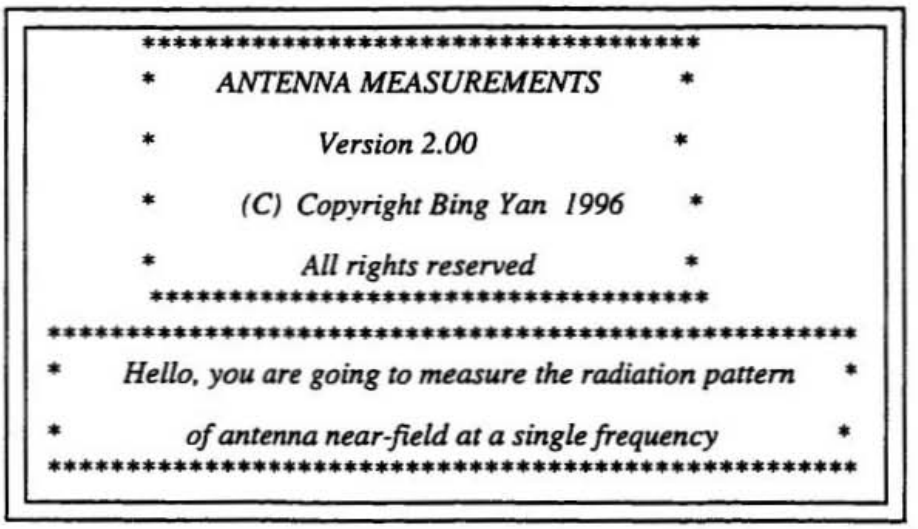

(2) Then, the PC will turn off the data drawing of VNA and select external measurement triggering, also CW turn on and CW frequency set to value:

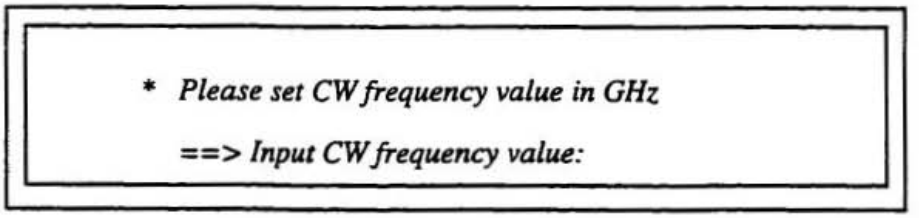

User inputs the value in GHz.

(3) After user inputs the frequency, program will ask you to select:

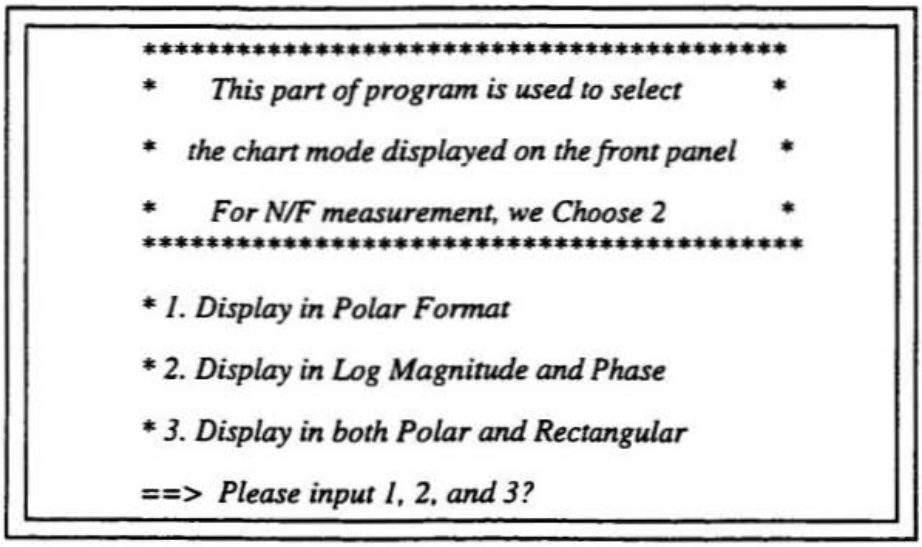

In near-field antenna measurement, we choose 2. If user choose other data not 1, 2, 3, then

" no choice! "

will appear on the screen.

(4) The PC will set the following information to VNA now

a) Set the display start from 0 and stop at 360 degree

b) Turn on data drawing

c) Active channel information

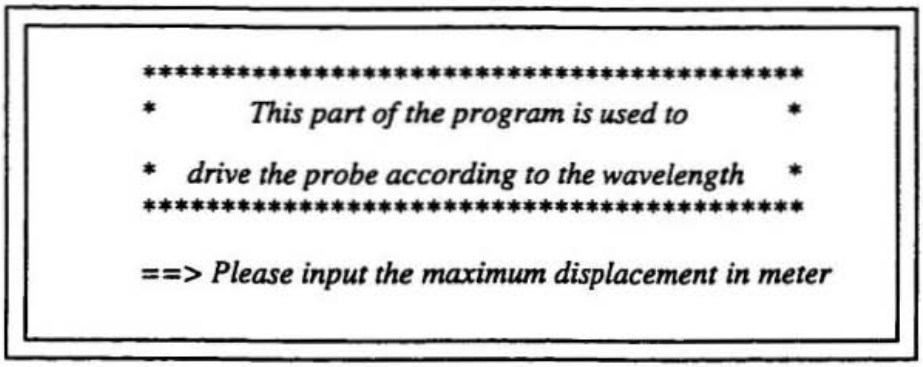

If the displacement inputted > 1.5m, it will ask the user to input again; otherwise it appears

==> Please input the factor (should be > or = 2):

After input the displacement you need, then it will calculate the number of turns according to the following relationship:

1 inch = 2.54 cm

0.25" × 20 threads per inch (Lloyd project)

turn = CINT(step-length/0.0254×0.25×20)

where the step-length is given by:

step-length = 0.3/frequency/factor

Also the number of points will be given by

points = CINT(displacement/step-length)

The number of turns in whole displacement is given by

counter = turn×(points-1)

Then all the information will appear on the screen:

** frequency =*

** the step-length is*

** turns in one step-length =*

** the number of points is*

** the number of turns in whole displacement =*

then it appears:

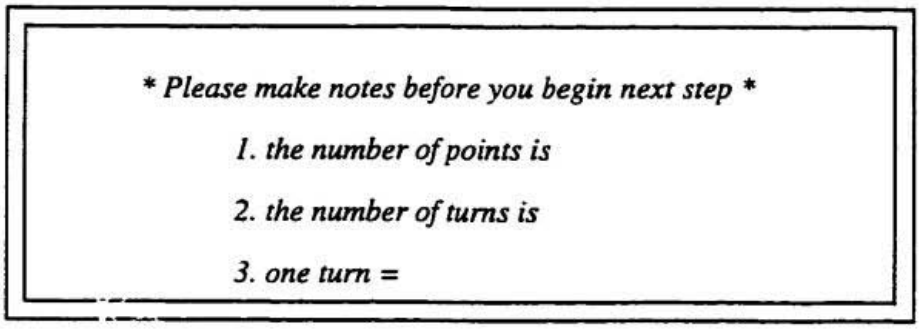

Then the PC will set the CW frequency calibration data points, also enter the number of points drawn in CW

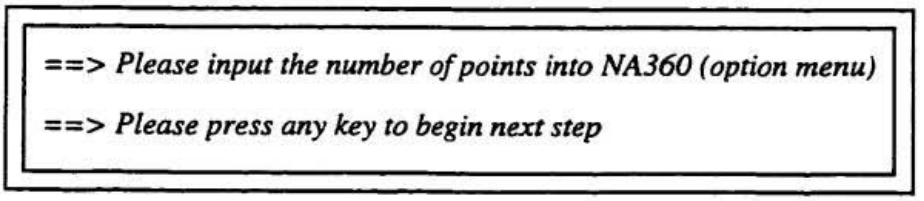

After all these operation, the PC will communicate with scanner.

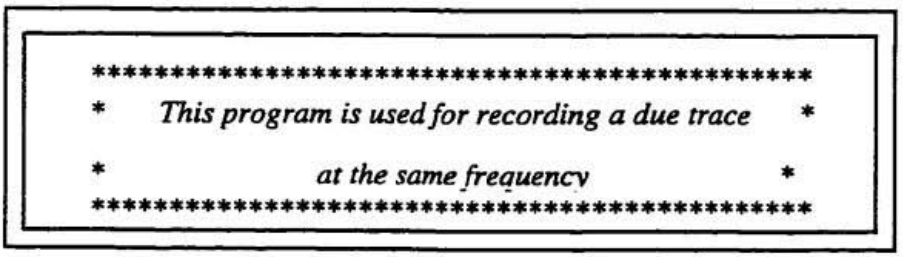

After all measurements have been done, the following information will appear on the screen

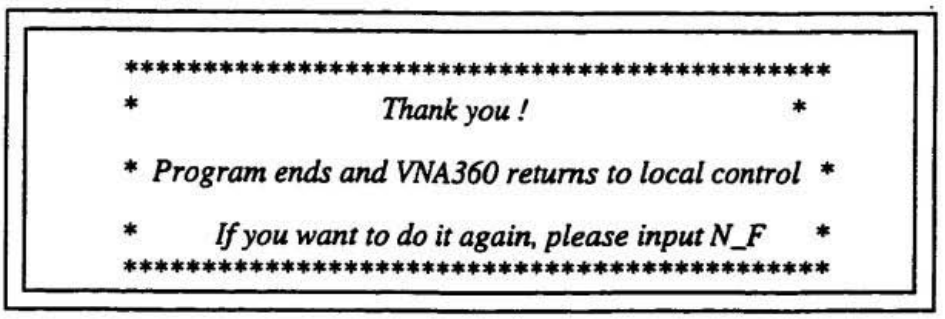

Note: Because the zero points are need to be measured, the points of probe pick up are odd.

Chapter 4

Near-Field to Far-Field Transformation

Since an antenna is a device for transforming a transmission guided wave into a wave radiated in space, or vice versa, and the distribution of field strength about an antenna is a function of both the distance from the antenna and the angular coordinates, the objective of this chapter is to determine antenna radiation patterns, and give the proper transformation of the far-field radiation pattern.

4.1 Far-field determination from source distributions derived from near-field measurements

Complete electric $\vec{E}$ and magnetic $\vec{H}$ fields within a given volume can be expressed in terms of the current densities of the sources within the volume and the values of the field itself over the boundaries of the volume. If the volume of interest is defined to contain no sources and to be bounded by a closed surface S and the sphere at infinity, the $\vec{E}$ and $\vec{H}$ fields at a point P within the volume are:

$$E_p = \frac{1}{4\pi}\int_s [-jwu(\hat{n}\times H)\psi + (\hat{n}\times E)\times\nabla\psi + (\hat{n}\cdot E)\nabla\psi da) \tag{4.1}$$

$$H_p = \frac{1}{4\pi}\int_s [-jwu(\hat{n}\times E)\psi + (\hat{n}\times H)\times\nabla\psi + (\hat{n}\cdot H)\nabla\psi da) \tag{4.2}$$

where $\hat{n}$ is the unit vector normal to the surface. The function ψ is the scalar portion of the Green's function and is given by

$$\psi = \frac{e^{-jkr}}{r} \tag{4.3}$$

where k is the free space wavenumber ($2\pi/\lambda$) and r is the distance from a point on the surface to a field point [6].

When it is desirable to determine the current or charge distribution on the surface of the antenna rather than the field distribution in an aperture, the closed surface S is assumed to be perfectly conducting and boundary conditions

$$\hat{n}\times E = 0 \qquad \hat{n}\times H = K$$

$$\hat{n}\cdot E = \frac{\rho_s}{\epsilon} \qquad \hat{n}\cdot H = 0 \tag{4.4}$$

are applied, where $\boldsymbol{K}$ is the surface current density and ρ_s is the surface charge density. If, in addition, the equation of continuity relating current density and charge density is utilized, the equations for the $\boldsymbol{E}$ and $\boldsymbol{H}$ fields can be expressed in terms of either current density or charge density alone. In terms of surface current density on the perfectly conducting surface S, the electric and magnetic fields at a point P in the volume of interest then can be expressed as

$$E_p = -\frac{j}{4\pi\omega\epsilon}\int_s [(K\cdot\nabla)\nabla + k^2 K]\frac{e^{-jkr}}{r} da \tag{4.5}$$

$$H_p = \frac{1}{4\pi}\int_s (K \times \nabla)\frac{e^{-jkr}}{r} da \qquad (4.6)$$

Thus, in its fundamental formulation, the method of determining field patterns from source distributions involves the application of (4.1, 2) for aperture distributions or (4.5, 6) for current distributions. In the first case, near-field measurements are made to determine the $\boldsymbol{E}$ and $\boldsymbol{H}$ field distributions over a surface surrounding the antenna [6]. Except for very simple geometries, (4.1-2, 5-6) are extremely difficult to apply without approximations. These approximations usually relate to the nature of the fields or currents on the surface over which the integration is performed. The approximations that are necessary to permit evaluation of the surface integrals usually fall into one of the following areas:

(1) Assuming negligible contribution of the fields or currents over some portion of the surface;

(2) Assuming all radiation follows outward normalize to the surface;

(3) Assuming the electric and magnetic fields are linearly related as in a plane wave;

(4) Assuming small-angle approximations and thus limiting the angular region for locating the field point.

Approximations of this type should be distinguished form the normal far-field approximations that simplify computation but produce valid results at distances sufficiently far from the source to satisfy far-field conditions.

4.2 Algorithm development--asymptotic evaluation of the aperture radiation field

The integral to be evaluated for large values of r is

$$\bar{E}(\bar{r}) = \frac{1}{4\pi^2}\int\int \bar{f}(k_x,k_y)e^{-j\bar{k}\cdot\bar{r}}dk_x dk_y \qquad (4.7)$$

The technique that will be used is Rayleigh's method of stationary phase. The rationale underlying this method is as follows: When r is very large $e^{-jk\cdot r}$ is a very rapidly oscillating function. Thus the contributions to the integral from various points in the $k_x k_y$ plane tend to cancel because there is a lack of in-phase addition from the various regions. An exception is a point where $\mathbf{k}\cdot\mathbf{r}$, which is a function of k_x and k_y, to first order does not vary with small changes in k_x, k_y. Such a point is called a stationary phase point and is characterized by the vanishing of the first derivatives of $\mathbf{k}\cdot\mathbf{r}$ with respect to k_x and k_y; that is,

$$\frac{\partial(\bar{k}\cdot\bar{r})}{\partial k_x} = 0 \qquad \frac{\partial(\bar{k}\cdot\bar{r})}{\partial k_y} = 0 \qquad (4.8)$$

At a stationary phase point the phase of $e^{-j\mathbf{k}\cdot\mathbf{r}}$ does not vary rapidly, and a nonzero contribution to the integral would be obtained from this region of the $k_x k_y$ plane. In the small region surrounding the stationary phase point, which we denote by $k_x=k_1$, $k_y=k_2$, the slowly varying function $f(k_x, k_y)$ is put equal to its value at the stationary phase point. The integral that remains then only involves the function $e^{-jk\cdot r}$ and can be evaluated.

In order to facilitate the evaluation we express $\bar{k}\cdot\bar{r} = k_x x + k_y y + k_z z$ in spherical coordinates by using $x = r\sin\theta\cos\phi$, $y = r\sin\theta\sin\phi$, $z = r\cos\theta$; thus

$$\bar{k}\cdot\bar{r} = r(k_x \sin\theta\cos\phi + k_y \sin\theta\sin\phi + \sqrt{k_0^2 - k_x^2 - k_y^2}\cos\theta) \tag{4.9}$$

The stationary phase point is the point where

$$\frac{\partial(\bar{k}\cdot\bar{r})}{\partial k_x} = 0 \qquad \frac{\partial(\bar{k}\cdot\bar{r})}{\partial k_y} = 0 \tag{4.10}$$

that is, where

$$k_x = k_1 = k_0 \sin\theta\cos\phi \tag{4.11-a}$$

$$k_y = k_2 = k_0 \sin\theta\sin\phi \tag{4.11-b}$$

A Taylor series expansion of $\bar{k}\cdot\bar{r}$ in vicinity of k_1, k_2 gives

$$\begin{aligned}\bar{k}\cdot\bar{r} &= k_0 r + \frac{1}{2}\frac{\partial^2\bar{k}\cdot\bar{r}}{\partial k_x^2}(k_x - k_1)^2 + \frac{1}{2}\frac{\partial^2\bar{k}\cdot\bar{r}}{\partial k_y^2}(k_y - k_2)^2 \\ &+ \frac{\partial^2\bar{k}\cdot\bar{r}}{\partial k_x\partial k_y}(k_x - k_1)(k_y - k_2) = k_0 r - (Au^2 + Bv^2 + Cuv)\end{aligned} \tag{4.12}$$

where $u = k_x - k_1$, $v = k_y - k_2$, and A, B, and C are constants defined by this equation.

The asymptotic solution for **E(r)** is thus

$$\bar{E}(\bar{r}) \sim \frac{e^{-jk_0 r}}{4\pi^2}\bar{f}(k_0\sin\theta\cos\phi, k_0\sin\theta\sin\phi)\iint_{\Delta s} e^{j(Au^2+Bv^2+Cuv)}\,du\,dv \tag{4.13}$$

where we have put **f** equal to its value at the stationary phase point, and Δs is a small region centered on the stationary phase point which is at $u=v=0$ in the uv phase. We now use the stationary phase argument again to note that $e^{j(Au^2+Bv^2+Cuv)}$ will oscillate very rapidly when u and v are not zero, since the constants A, B, C are proportional to r and consequently very large for large values of r. Thus the integral can be extended to cover the whole uv plane, since in the limit

as r becomes infinite the contributions from u and v outside of Δs will cancel from phase interference. Hence we need to evaluate the following expression:

$$\int\int_{-\infty}^{\infty} e^{j(Au^2+Bv^2+Cuv)}dudv \tag{4.14}$$

Because

$$Au^2 + Bv^2 + Cuv = (\sqrt{A}u + \frac{Cv}{2\sqrt{A}})^2 - \frac{C^2v^2}{4A} + Bv^2$$

and put $\sqrt{A}u + (Cv/2\sqrt{A}) = w$ to get for the integral the result

$$I = \int\int_{-\infty}^{\infty} e^{jw^2} e^{j(4AB-C^2)v^2/4A} \frac{dw}{\sqrt{A}}dv$$

Next we use the known result

$$\int_{-\infty}^{\infty} e^{j\gamma(x-x_0)^2}dx = \sqrt{\frac{\pi}{\gamma}}e^{j\pi/4} \tag{4.15}$$

to evaluate the integrals over w and v. We then obtain

$$I = \frac{j2\pi}{\sqrt{4AB-C^2}} = 2\pi j\frac{k_0}{r}\cos\theta$$

upon using

$$A = \frac{r}{2}(\frac{1}{k_0} + \frac{k_1^2}{k_0^3\cos^2\theta})$$

$$B = \frac{r}{2}(\frac{1}{k_0} + \frac{k_2^2}{k_0^3\cos^2\theta})$$

$$C = \frac{k_1k_2r}{k_0^3\cos^2\theta}$$

Our final result is [25]

$$\bar{E}(\bar{r}) \sim \frac{jk_0 \cos\theta}{2\pi r} e^{-jk_0 r} \bar{f}(k_0 \sin\theta\cos\phi, k_0 \sin\theta\sin\phi) \tag{4.16}$$

with

$$\bar{f}_t(k_x, k_y) = \iint_{S_a} \bar{E}_a(x, y) e^{jk_x x + jk_y y} dxdy \tag{4.17}$$

Equation (4.8) and (4.9) will be used to get the far-field radiation patterns.

4.3 FFT Algorithm used for far-field

In a source-free region in which near-fields are measured, the time-harmonic Maxwell equations can be transformed into:

$$\nabla\bar{E} + k^2\bar{E} = 0$$

$$\nabla\bar{H} + k^2\bar{H} = 0$$

$$\nabla \cdot \bar{E} = \nabla \cdot \bar{H} = 0$$

The far-zone radiation field computed from the aperture electric field is given by [25]

$$\bar{E} = \frac{jk_0}{2\pi r} e^{-jk_0 r} [a_\theta (f_x \cos\phi + f_y \sin\phi) + a_\phi (f_y \cos\phi - f_x \sin\phi)\cos\theta] \tag{4.18}$$

where the following fast Fourier transforms (FFT) are used:

$$f_x(k_x, k_y) = \int_{S_a} E_{ax}(x, y) e^{jk_x x + jk_y y} dxdy \tag{4.19-a}$$

$$f_y(k_x, k_y) = \int_{S_a} E_{ay}(x, y) e^{jk_x x + jk_y y} dxdy \tag{4.19-b}$$

and $k_x = k_0 \sin\theta\cos\phi$, $k_y = k_0 \sin\theta\sin\phi$.

Since the measured near-field data are discrete, i.e. not continuos, the equation (19-a, b) become:

$$f_x(k_x,k_y)=\sum_{i=1}^{n}\sum_{j=1}^{n}E_{ax}(x_i,y_j)e^{jk_x x_i+jk_y y_j}\Delta x\Delta y \qquad (4.20\text{-a})$$

$$f_y(k_x,k_y)=\sum_{i=1}^{n}\sum_{j=1}^{n}E_{ay}(x_i,y_j)e^{jk_x x_i+jk_y y_j}\Delta x\Delta y \qquad (4.20\text{-b})$$

where $E_{ax}(x_i,y_j)$ and $E_{ay}(x_i,y_j)$ are the E_x and E_y components what we measured in position (x_i, y_j) on the near-field planar, which include magnitude and phase components, as shown in Figure 4.1.

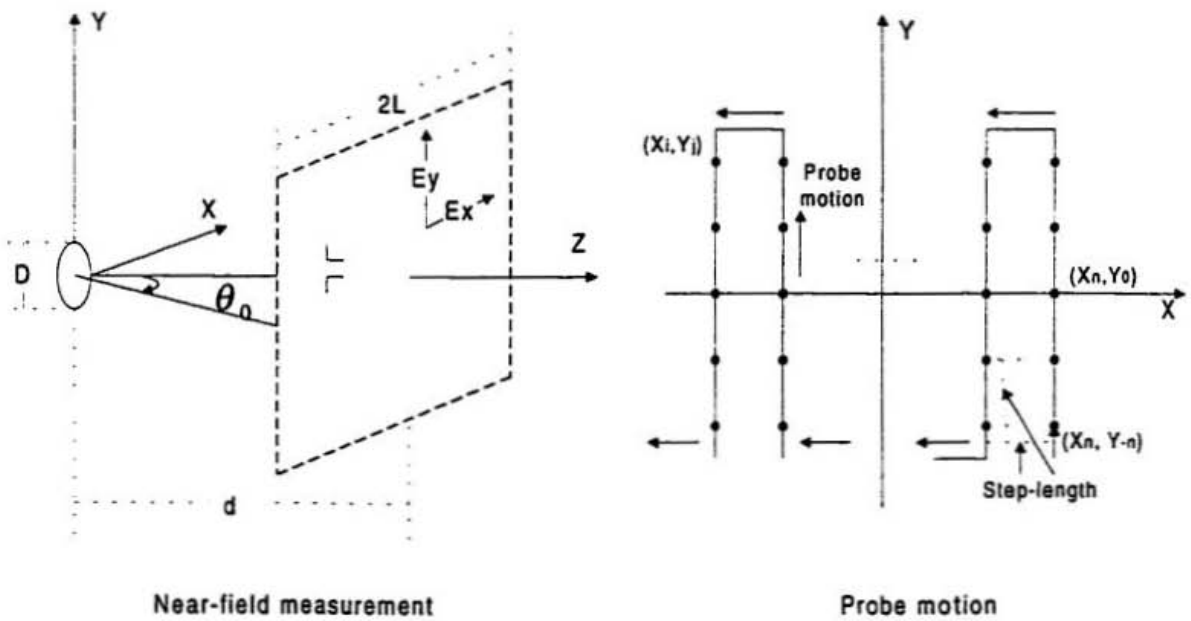

Figure 4.1 Near-field measurement
Ex, Ey, and step-length

$$E_{ax}(x_i, y_j) = |E_{ax}(x_i, y_j)| e^{jk\varepsilon_{xphase}} \quad (4.21\text{-a})$$

$$E_{ay}(x_i, y_j) = |E_{ay}(x_i, y_j)| e^{jk\varepsilon_{yphase}} \quad (4.21\text{-b})$$

Δx and Δy are equal to step-length

$$\Delta x = \Delta y = \frac{\lambda}{factor} \quad (factor \geq 2) \quad (4.22)$$

After submitting these definitions, we can get far-field radiation patterns from equation (21-a & 21-b).

In fact, the network analyzer measures gain instead of $\boldsymbol{E}$. When we apply the FFT algorithm to get far-field radiation patterns, we use the following equation in programming:

$$P \sim E^2$$

It is because of

$$P = \vec{E} \times \vec{H}$$

and outside of the reactive (evanescent) near-field region, the E and H fields are related by the characteristic impedance of free space (377Ω) [2].

4.4 Algorithm application

After the near-field measurement has been performed, the next step is to use the algorithm described alone to calculate the far-field radiation pattern. The following flowchart in Figure 4.2 describes the operation in detail.

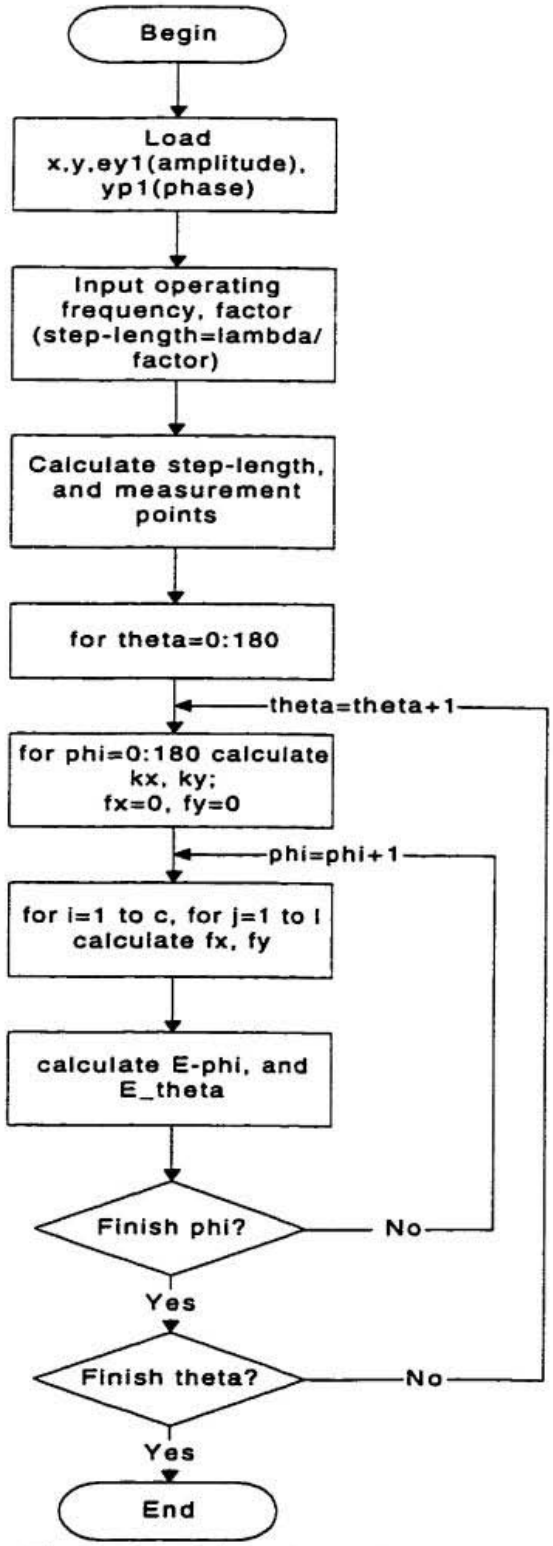

Figure 4.2 Flowchart of near-field/far-field transformation

4.5 One dimensional near-field antenna measurement

The One dimensional near-field antenna measurement develops from the general equation which is based on the aperture electric far-field radiation pattern is given by (4.18). In most conditions, we are only interested in the normalized horizontal antenna radiation patterns, as shown in Figure 4.3.

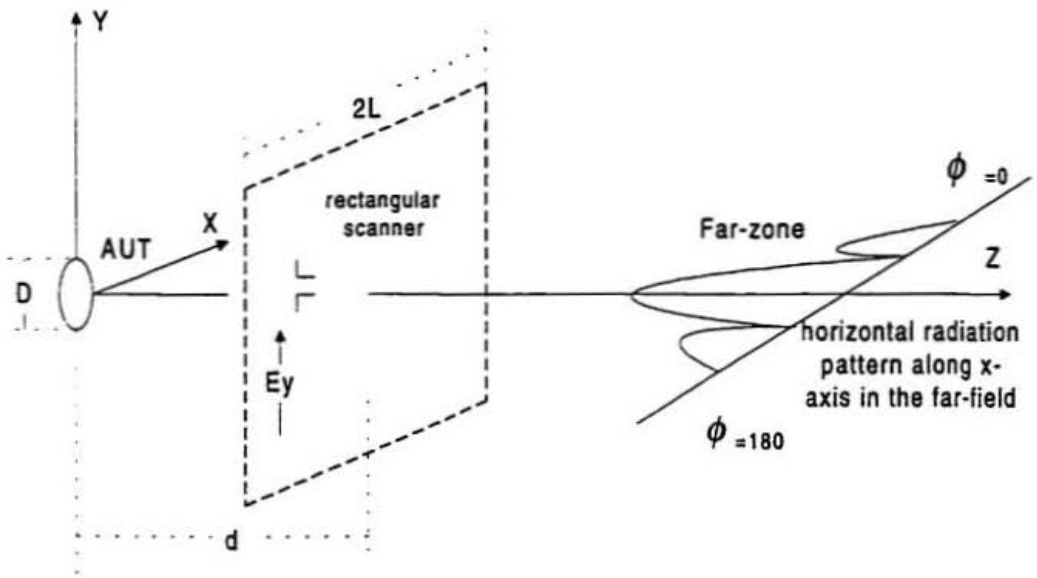

Figure 4.3 One-dimensional near-field measurement

In this case, $\phi = 0^{\circ}$ or $\phi = 180^{\circ}$ are used. So, equation (4.18) can be rewritten into

$$E_{\phi=0} = \frac{jk_0}{2\pi r} e^{-jk_0 r} [a_\theta (f_x \cos 0 + f_y \sin 0) + a_\phi (f_y \cos 0 - f_x \sin 0) \cos\theta]$$

$$E_{\phi=180} = \frac{jk_0}{2\pi r} e^{-jk_0 r} [a_\theta (f_x \cos 180 + f_y \sin 180) + a_\phi (f_y \cos 180 - f_x \sin 180) \cos\theta]$$

from which we get

$$E_{\phi=0} = \frac{jk_0}{2\pi r} e^{-jk_0 r} [a_\theta f_{x_0} + a_\phi f_{y_0} \cos\theta] \tag{4.23-a}$$

$$E_{\phi=180} = \frac{jk_0}{2\pi r} e^{-jk_0 r} [-a_\theta f_{x_{180}} - a_\phi f_{y_{180}} \cos\theta] \tag{4.23-b}$$

where

$$f_{x_0} = \sum_{i=1}^{n} E_{ax}(x_i, 0) e^{jk_0 \sin\theta x_i} \Delta x$$

$$f_{y_0} = \sum_{i=1}^{n} E_{ay}(x_i, 0) e^{jk_0 \sin\theta x_i} \Delta x$$

$$f_{x_{180}} = \sum_{i=1}^{n} E_{ax}(x_i, 0) e^{-jk_0 \sin\theta x_i} \Delta x$$

and we can get

$$\left| f_{x_{00}} \right| = \left| f_{x_{180}} \right|$$

$$\left| f_{y_0} \right| = \left| f_{y_{180}} \right|$$

$$|E_{\phi=0}| = |E_{\phi=180}| = \left| \frac{k_0 e^{-jk_0 r}}{2\pi r} \right| |a_\theta f_{x_0} + a_\phi f_{y_0} \cos\theta| \tag{4.24}$$

4.6 Probe-correction for planar near-field scanning

When near-field antenna measurements are performed, the collected data are the received power of a probe, which has a known near-field receiving radiation pattern, results from scanning on a plane in front of the AUT. The assumes that the probe receives with ominidirectional capability and that multiple interactions between the probe and the test antenna are negligible [18].

In fact, the probe used in our measurements is a dipole antenna which has a specific near-field parameters. Probe-correction is not required for on-axis gain comparison measurements. The probe-correction affects gain only at off-axis angles. Most antenna gain measurements are made on boresight, requiring no probe-correction. Multibeam antenna gain measurements usually require probe-correction. Probe-correction, however, is required for directly measurements [40]. When one focuses on the boresight antenna gain measurements, we do not consider the effect of probe-correction. When we do other off-axis angles measurements, probe-correction needs be taken into account.

The far-field pattern of the test antenna is the Fourier transform of the output of the probe divided by the far-field pattern of the probe [18]. The final probe-correction formula is given by equation (25).

$$\overline{\overline{T}}_0(k_x,k_y)=\frac{e^{-i\gamma z_0}}{(2\pi)^2 a_0}\overline{\overline{R}}_P^{-1}(k_x,k_y)\cdot\int_{-\infty}^{+\infty}\int_{-\infty}^{+\infty}\overline{b}_p(\overline{r}_0)e^{-i(k_x x_0+k_y y_0)}dx_0dy_0 \quad (25)$$

The spectrum $\overline{\overline{T}}_0$ is represented for the electric field radiated into free space by the test antenna as a product of the inverse receiving characteristic of the probe and the Fourier transform of the vector output of the probe [18].

In our measurement, one-dimensional near-field antenna measurement is preferred. It is an on-axis measurement and does not need to consider of probe correction.

Chapter 5

Validation of the System

Several preliminary, one-dimensional tests were performed to find the required near-field spacing and scan size, the best value of the probe-antenna-separation distance, and to find the level of the leakage, and to reduce it, if necessary. Comparisons with the far-field radiation patterns obtained by direct measurement inside C-CORE's RF anechoic chamber will determine the success of the developed near-field/far-field measurement system.

5.1 Description of Antenna under test

In the tests, we use two different antennas as the AUT: one is an L/C band microstrip antenna which was designed and built following specification set by the Canadian Space Agency (CSA) for satellite-based Synthetic Aperture Radars (SAR's); the other is a horn antenna.

5.1.1 L/C band microstrip antenna

The CSA specifications for an L/C band microstrip antenna requires operation in both the L band at 1.275 GHz and in the C band at 5.3 GHz. This antenna was designed, built and tested

inside C-CORE's RF anechoic chamber [26]. The antenna specifications are described in Table 5.1:

Table 5.1 Device Specifications

	C-Band	L-Band
Frequency	5.3 GHz	1.275 GHz
Bandwidth	10 MHz	10 MHz
Radiation pattern	Broadside	Broadside
Polarization	Dual Linear	Dual Linear

The antenna shape and size is shown as Figure 5.1 and Figure 5.2.

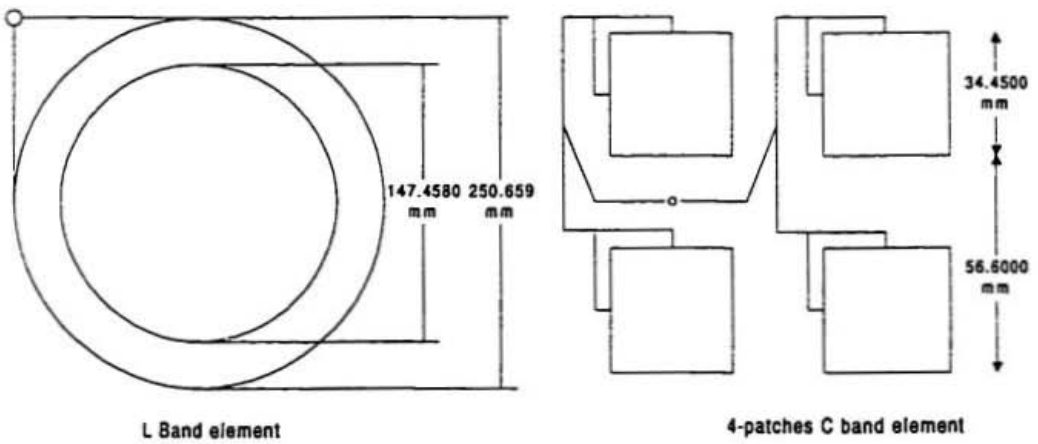

Figure 5.1 L/C band Microstrip antenna elements

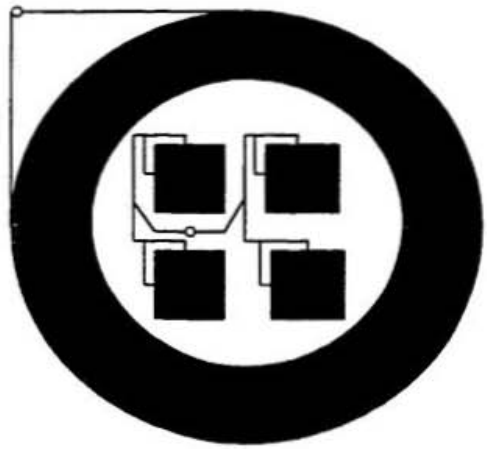

Figure 5.2 L/C microstrip antenna

5.1.2 Horn antenna

The horn antenna used here is a commercial antenna. Its structure is shown as Figure 5.3.

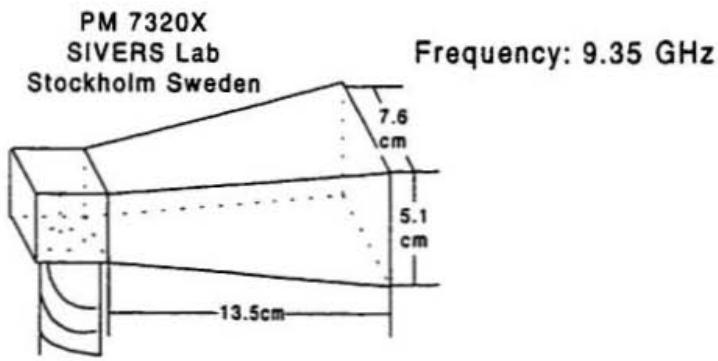

Figure 5.3 Antenna under test
horn antenna

The operating frequency is 9.35 GHz.

5.2 Test sample spacing

The test-sample-spacing procedure was used to find the required near-field spacing. It consisted of taking one-dimensional scans in x and y with very fine spacing (about 0.25λ). First, an FFT was performed on the full set of data, then using only every other point, then using every third point, and so forth. From this, we could compare the far-field spectra from various spacings. The smallest spacing was assumed adequate. When the spacing from the other FFTs was so large that the spectrum changed by more than the desired accuracy, a spacing equal to or smaller than the next smallest spacing was used.

From these one-dimensional tests, we concluded that the spacing between near-field data points should have been about 0.5λ for the L band and 0.24λ for the C band for microstrip antenna; and 0.5λ for the horn antenna, in both x and y, where λ was changed according to different band.

5.3 Test scan-length and distance

In principle, the planar near-field method assumes measurements on an infinite plane. Since this is impossible, we had to determine the required scan size to obtain the desired accuracy over the angular region of interest. This scan-area truncation had two effects. First, the far-field results were valid only within the angular region θ_0 defined by the AUT aperture and the scan area as shown in Figure 5.4.

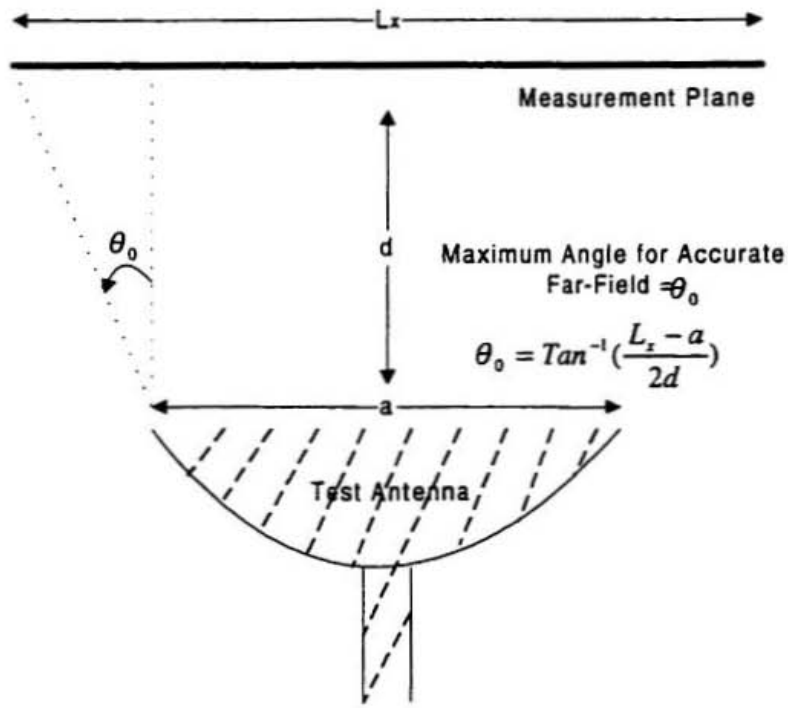

Figure 5.4 A schematic showing the angle of validity of the far-field, based on the near-field geometry.

Second, truncation produced errors within the region of validity because the field was non-zero at the edge of the scan area. This non-zero amplitude caused a small ringing when the FFT was performed.

The test-scan-length procedure was similar to the test-sample-spacing procedure, in that one-dimensional centerline scans in x and y were performed. These centerline scans were very long, and data were truncated from the edge in various amounts. As in the test-sample-spacing procedure, the computed spectra were compared, and a required scan-length was determined. In our test, scan-length is less than *1.5m*. For L band microstrip antenna, the scan-length is about *1.2m*; for C band microstrip antenna, the scan-length is about *0.5m*; for horn antenna, the scan-length is about *0.41m*.

The distance between the AUT and the scanning plane is selected in the range of $2\pi/\lambda$~10λ.

5.4 Probe selection

In our test, we have used three small antennas as probes. They are monopole, dipole, and small horn antenna. After using the FFT, we found the near-field measured by the small dipole is the best because it causes less reflection than the horn antenna, and it is easier to conform the center than the monople antenna. Its shape and size are shown in Figure 5.5. For L band microstrip antenna, far-field radiation patterns calaculated from near-field measurements obtained by different probes are shown in Figure 5.6. Small dipole probe is recommanded because the far-field radiation pattern obtained from its measurement matches the direct far-field radiation pattern obtained inside C-CORE's RF anechoic chamber.

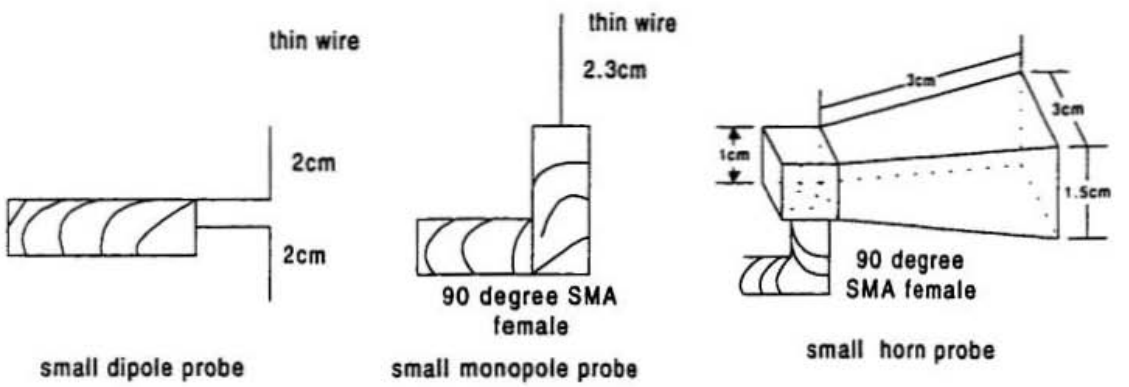

Figure 5.5 Probes used in tests

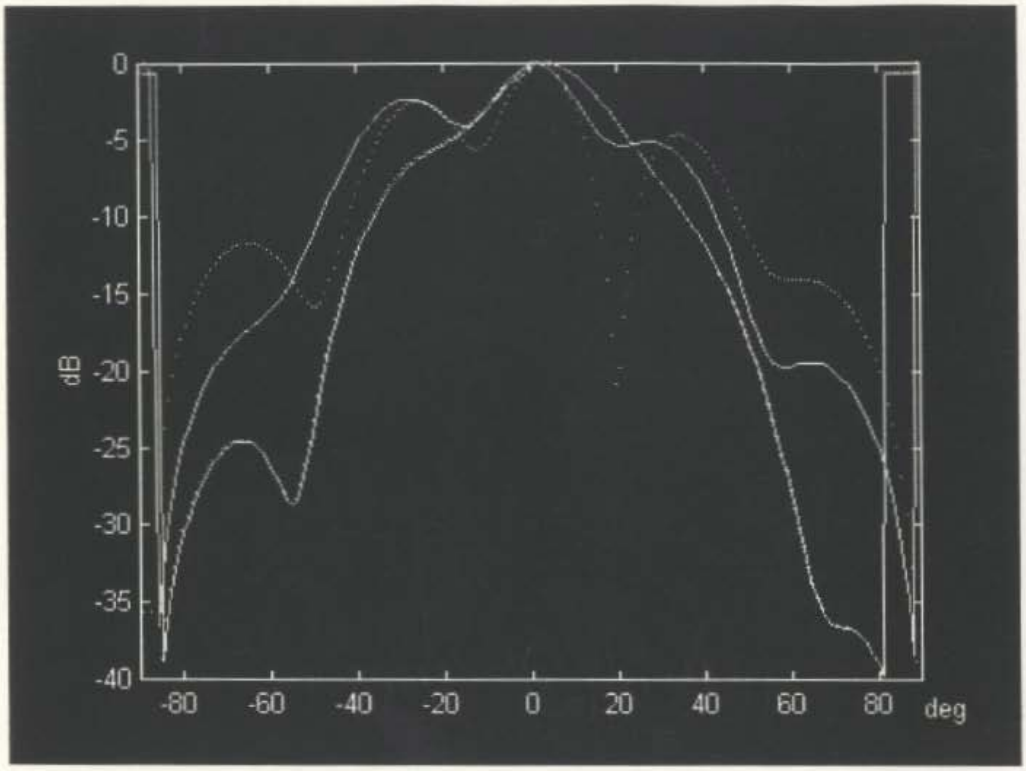

Figure 5.6 Comparison of different probes measurement results

In Figure 5.6 "." line represents the far-field radiation pattern calculated from the near-field which is measured by the small horn antenna; "-" line represents the far-field radiation pattern calculated from the near-field which is measured by the small dipole antenna;"./-" line represents the far-field radiation pattern calculated from the near-field which is measured by the small monopole antenna.

5.5 Test results

During the measurements, different distances from the AUT have been applied, and different sampling length have been selected. For different AUT, different results are given.

5.4.1 Test results for L/C band microstrip antenna

When we put the L/C band microstrip AUT, the key characteristics are given in Table 5.2:

Table 5.2 Near-field measurement characteristics (Microstrip antenna)

	C-Band	L-Band
Operating frequency	5.79 GHz	1.29 GHz
Probe shape & size	4cm dipole	4cm dipole
Distance between probe & AUT(d)	13 cm	30 cm
Number of discrete points	19 ×19	9× 9
Grid size	0.466 m	1.213 m
θ_0	32.6°	56.69°

where θ_0 is the largest angel from broadside direction with accurate results as shown in Figure 5.4 before. After near-field measurement, we apply the FFT transformation to get far-field radiation patterns. It is shown as Figure 5.7.

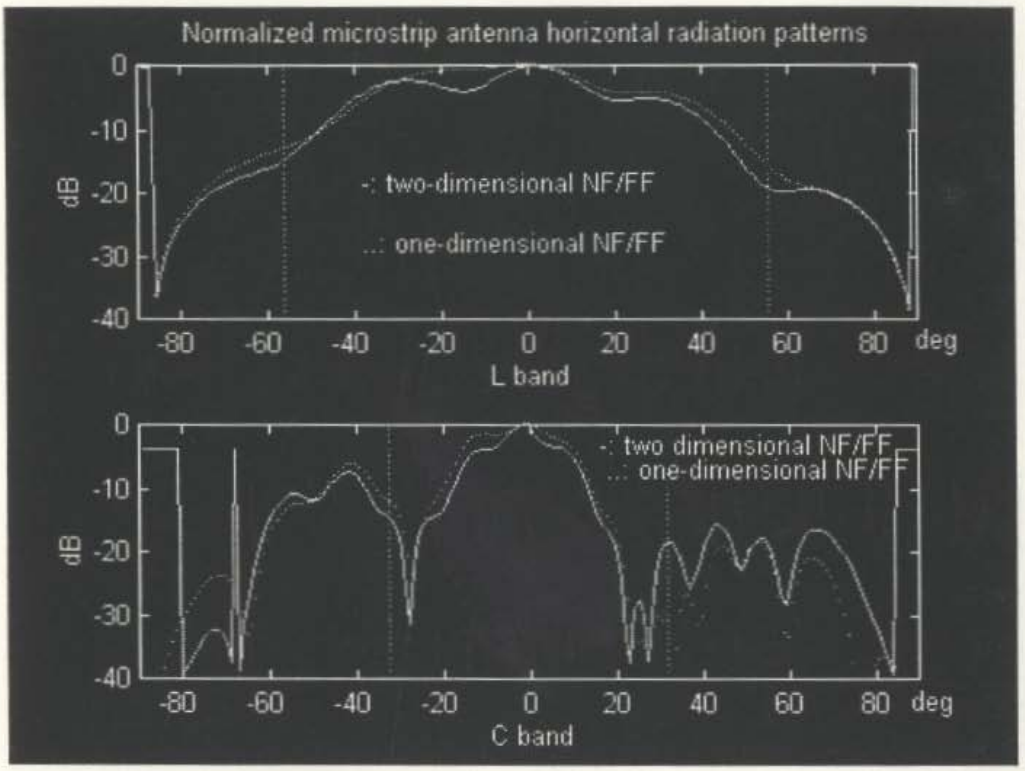

Figure 5.7 Far-field radiation patterns of microstrip antenna

(calculated by two-dimensional and one-dimensional NF/FF measurement)

5.5.2 Test results for horn antenna

Other antennas have been used as AUT, such as the horn antenna which has a operation frequency of *9.35 GHz*. Its characteristics are listed in Table 5.3:

Table 5.3 Near-field measurement of horn antenna

Operating frequency	9.35 GHz
Probe shape & size	4cm dipole
Distance between probe & AUT (d)	22 cm
Number of points	29 ×29
Grid size	0.41 m
θ_0	39.2°

Figure 5.8 gives the far-field radiation patterns calculated by one-dimensional and two-dimensional near-field measurements.

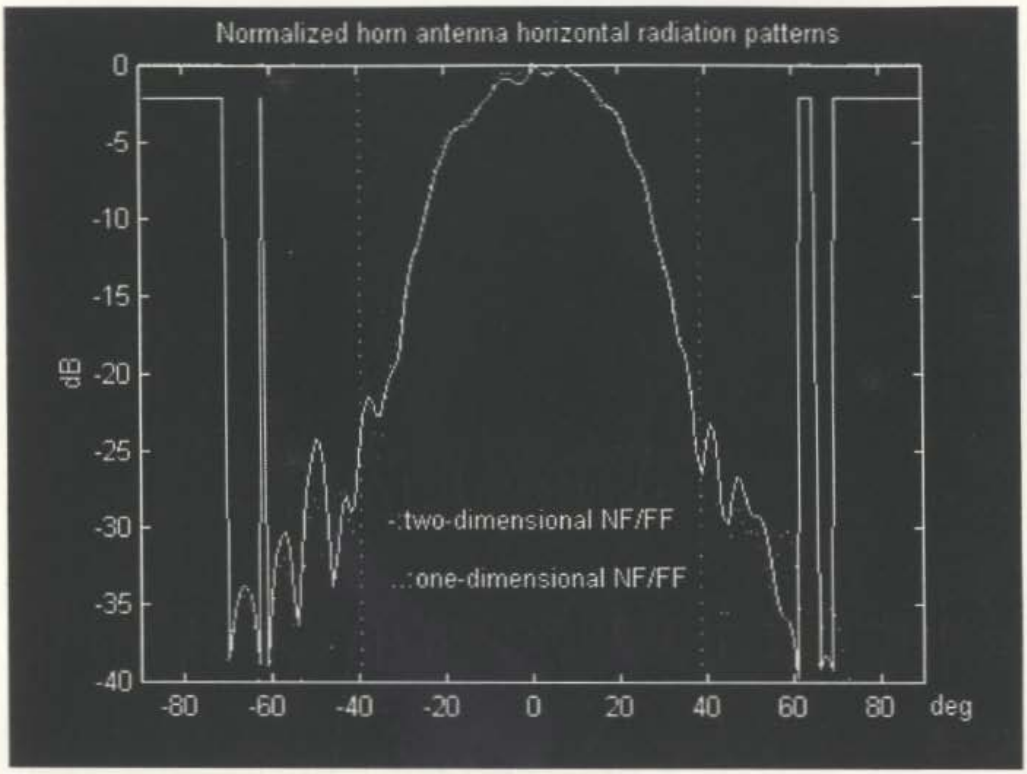

Figure 5.8 Far-field radiation pattern of horn antenna

5.6 Comparison of the direct far-field

After near-field antenna measurements have been performed, FFT is used to obtain the far-field radiation patterns. The far-field radiation patterns from near-field/far-field antenna measurement need to be evaluated by direct far-field measurement results. An anechoic chamber measurement system in C-CORE, MUN, are used to validate this.

5.6.1 Anechoic chamber measurement system

The direct far-field radiation patterns of the two antennas are measured inside C-CORE's anechoic chamber. Direct measurements of the far-field inside the chamber were performed by a transmitter antenna in the shape of a small log-period ground based dipole antenna. The AUT was placed on a rotating table at the other end of the chamber. The VNA outside the chamber measured the power transmitted between the two antennas when the AUT rotated [26]. The anechoic chamber is a $4m \times 2.5m \times 2.5m$ metallic box covered by radio frequency absorbers. The AUT is mounted on a rotating table inside the chamber, and the transmitter antenna is a log-periodic antenna. The distance between the AUT and the transmitter is about 2.4m. We measured the horizontal radiation pattern of the microstrip antenna $\pm 90°$ from the broadside direction. Figure 5.9 shows the anechoic chamber measurement system at C-CORE.

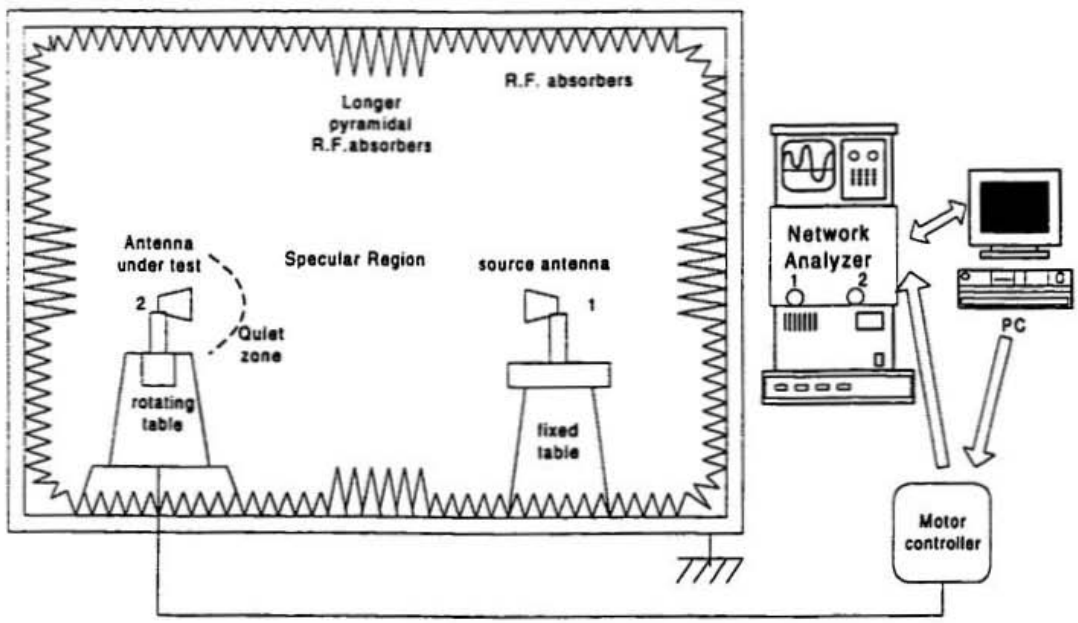

Figure 5.9 Anechoic chamber measurement system

The computer will drive the motor controller to rotate the table and record the measurement from the VNA. The VNA we used is a two-port Wiltron product Model 360 which has a frequency range of *40MHz - 40GHz* and frequency resolution of *100KHz*. The motor controller is the NF90 stepping motor controller which is produced by Velmex Inc.. The communication between the PC and the motor controller is performed by RS-232. Quickbasic embedded assembly language is used in programming.

5.6.2 Comparison of near-field and far-field results

One can compare the far-field patterns obtained from the low cost near-field antenna measurement system built in C-CORE with those obtained by the anechoic chamber measurement system in C-CORE. When we plot them together as shown in Figure 5.10, we found that the difference between the two patterns was generally less than *5 dB* in validity range, which is rather acceptable. Furthermore, when one compares one-dimensional antenna near-field measurement results with the other two, as shown in Figures 5.10, 5.11, 5.12, the difference between them and the data measured inside the anechoic chamber are even less. One can attribute this to the fact that the dipole is more omnidirectional as it travels horizontally parallel to the AUT than when it moves. The changes in the dipole gain when it travels vertically can be considered as the reason for the departure of the grid model far-field pattern from the direct far-field since probe correction methods have not been implemented here. Figure 5.10 and Figure 5.11 give the comparison of the L/C band microstrip antenna horizontal radiation pattern; and Figure 5.12 gives the comparison of horn antenna horizontal radiation patterns.

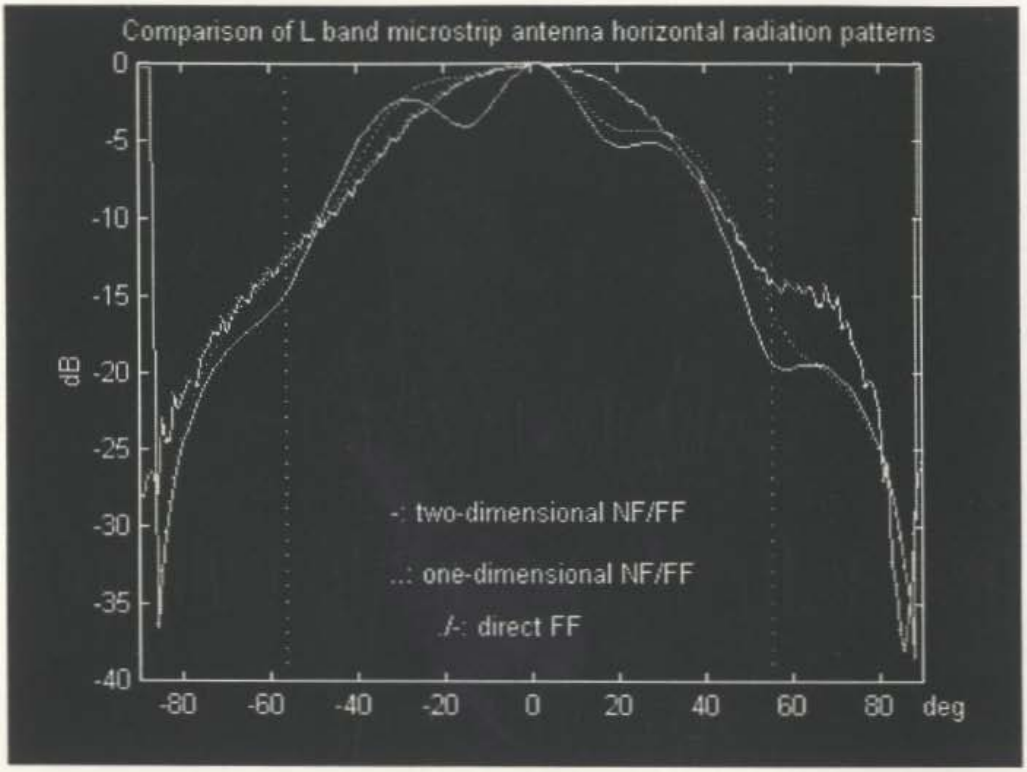

Figure 5.10 Comparison of L band microstrip antenna horizontal radiation pattern

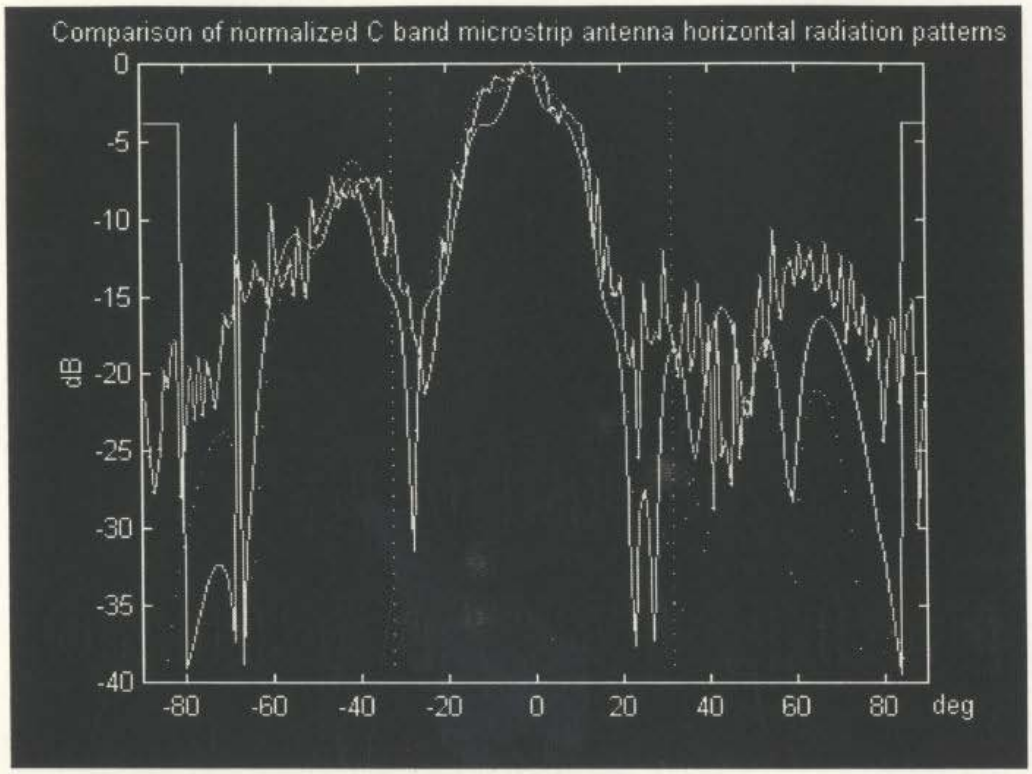

Figure 5.11 Comparison of C band microstrip antenna horizontal radiation pattern

In Figure 5.11 "./-" represents direct far-field radiation pattern measured inside anechoic chamber measurement system; "-" represents far-field developed from 2-dimensional near-field antenna measurement; "." represents far-field developed from one-dimensional near-field antenna measurement.

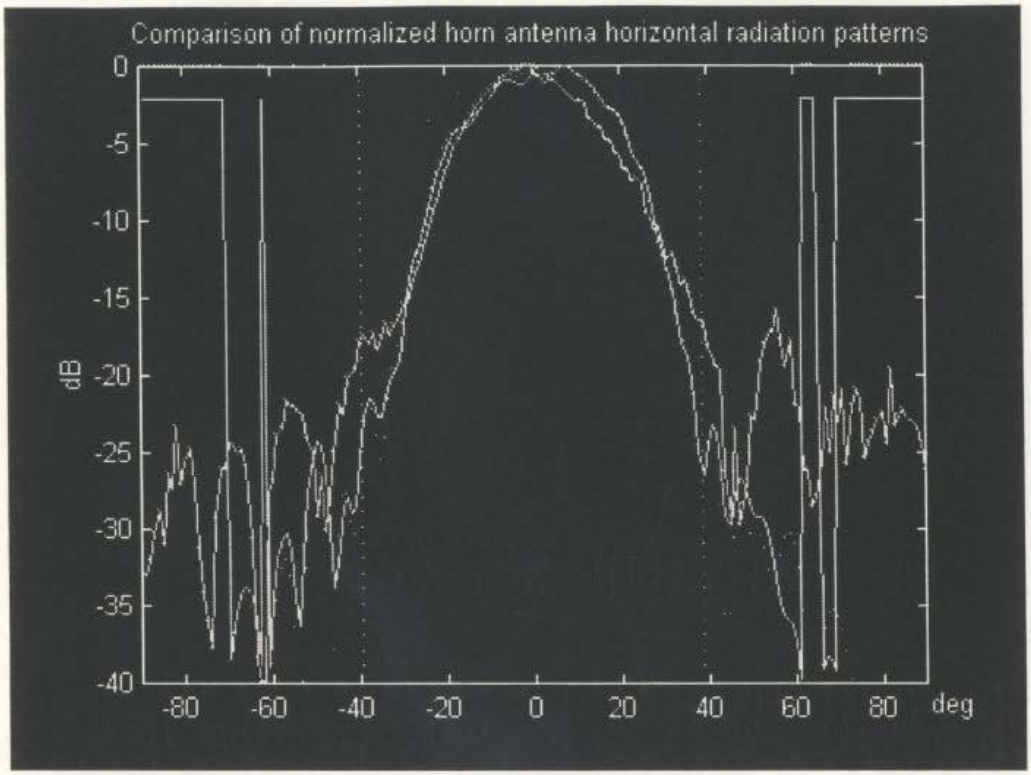

Figure 5.12 Comparison of horn antenna horizontal radiation pattern

In Figure 5.12 "./-" line represents direct far-field radiation pattern measured inside anechoic chamber measurement system; "-" line represents far-field developed from 2-dimensional near-field antenna measurement; "." line represents far-field developed from one-dimensional near-field antenna measurement.

5.7 Recommendation

The effect of the multiple interactions can formally be taken into account by using the plane-wave scattering-matrix theory [18], but in our test, we assume the distance between the probe and the test antenna is always large enough for multiple interactions between the test antenna and the probe to be negligible. In order to reduce the multi-reflection during measurements, low power of VNA is recommended. In our test, 0.0dBm power is used.

Different position of AUT causes different near-field antenna measurement results, and cause different far-field data. Figure 5.13, 5.14 show the different positions we used for the L/C band microstrip antenna near-field measurements; position 1 is preferred.

The difference between direct and indirect antenna measurement data may be caused by different probes we used for different system, and also different cables.

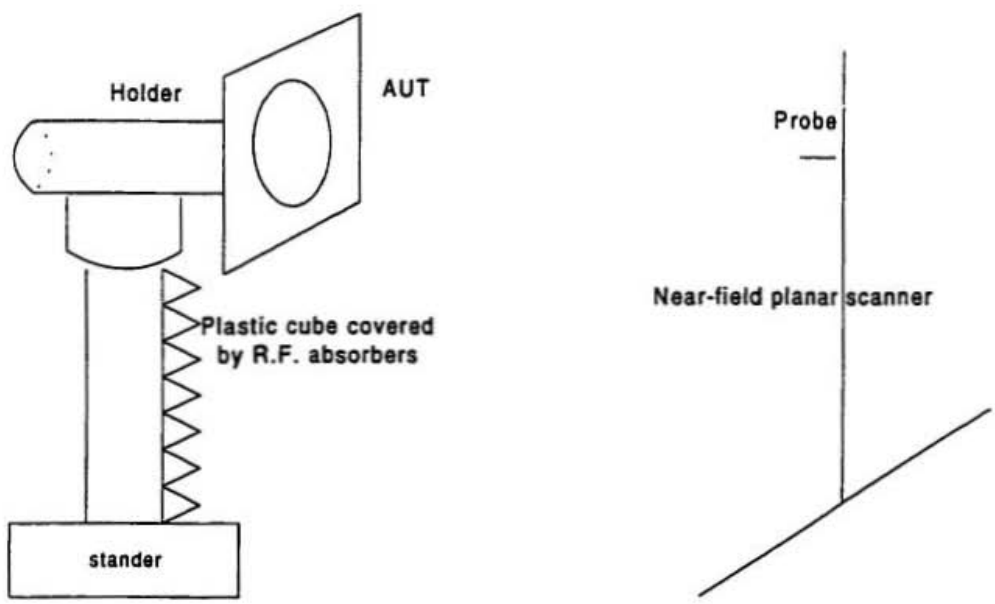

Figure 5.13 Near-field antenna measurement: position 1

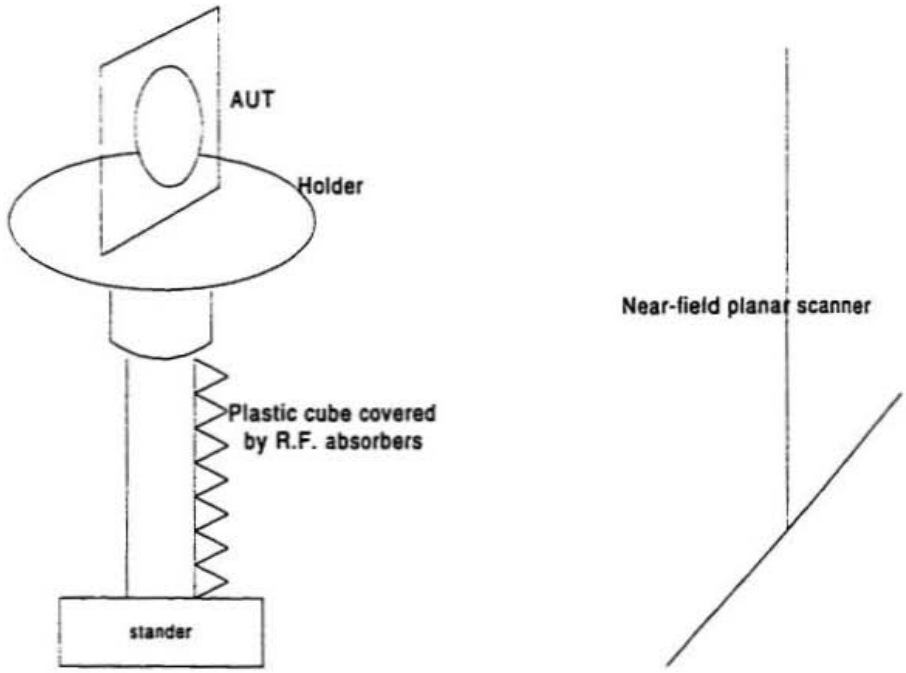

Figure 5.14 Near-field antenna measurement: position 2

Chapter 6

Conclusion and Future Works

6.1 Conclusion

A low cost near-field/far-field antenna measurement system has been designed, built in C-CORE, Memorial University of Newfoundland. Validating was done by using direct far-field antenna measurement system (C-CORE's anechoic chamber measurement system). One- and two-dimensional near-field measurements are performed on the planar scanning plane in the near-field. FFT algorithm is used in the development of the far-field radiation pattern. Reasonable agreements are observed between the data calculated from the near-field/far-field measurement and direct far-field data measured in C-CORE's anechoic chamber measurement system.

One-dimensional near-field antenna measurements are preferred when measuring horizontal radiation patterns. One-dimensional near-field antenna measurements do not need probe-correction, also they make the near-field/far-field measurement speed and data process speed fast comparing with two-dimensional near-field measurement.

The data obtained from near-field/far-field measurements and those directly measured inside the chamber validate both techniques.

The software package for the system is written in such a way that it has a user friendly interface.

6.2 Future works

All of the near-field measurement results we obtained, are performed outside of the chamber. If measurements are performed inside the chamber, the near-field measurement results should be better.

The far-field radiation patterns which are obtained from two-dimensional near-field measurements do not apply probe correction. Probe correction can be considered in the future works.

References

[1] Yahya Rahmat-Samii and Mark S. Gatti, " Far-field patterns of spaceborne antennas from plane-polar near-field measurements", IEEE trans. on Antennas and propagation, Vol. Ap-33, No.6, pp. 638-648, June 1985.

[2] Dan Slater, "Near-field antenna measurements", Artech House, Inc., 1991.

[3] Gary E. Evans, "Antenna measurement techniques", Artech House, Inc., 1990.

[4] Thorkild B. Hansen, and D. Yaghjain, "Planar near-field scasnning in the time domain, Part 1: Formulation",IEEE Trans. on Antenna and Propagation, Vol. 42, No. 9, September 1994,

[5] Arthur D. Yaghjian, "An overview of near-field antenna measurements", IEEE trans. on antenna and propagation, Vol. AP-34, No. 1, pp. 1280-1291, January 1986.

[6] Richard C. Johnson, H. Allen Ecker, and J. Searcy Hollis, "Determination of far-field antenna patterns from near-field measurements", Proc. of The IEEE, Vol. 61, No. 12, pp. 1668-1694, December 1973.

[7] Yahya Rahmat-Samii, Lawrence I. Williams, and Robert G. Yaccarino, "The UCLA bi-polar planar-near-field antenna measurement and diagnostics range", IEEE Antenna & Propagation Magazine, Vol. 37, No. 6, December 1995.

[8] Y.T. Lo & S.W. Lee, "Antenna handbook", Volume IV, Chapman & Hall, New York, NY, 1993.

[9] Y.T. Lo & S.W. Lee, "Antenna handbook", Volume I, Chapman & Hall, New York, NY, 1993.

[10] E. S. Gillespie, "Measurement of antenna radiation characteristics on far-field ranges", in *Antenna handbook*, Edited by Y.T.Lo & S.W.Lee, Van Nostrand Reinhold Company, New York, 1993.

[11] "IEEE Standard Test Procedures for Antenna", The Institute of Electrical and Electronics Engineers, Inc., 1979.

[12] Paul F. Wacker, "Unified theory of near-field analysis and measurement: nonmathematical discussion", IEEE Trans. on antenna and propagation, Vol. AP-30, No. 1, pp. 99-107, January 1982.

[13] Johnson J. H. Wang, "An examination of the theory and practices of planar near-field measurement", IEEE Trans. on antenna and propagation, Vol. 36. No. 6, pp. 746-753, June 1988.

[14] Edward B. Joy and Demetrius T. Paris, "Spatial Sampling and filtering in near-field measurements", IEEE Trans. on Antenna and propagation, Vol. AP-20, No. 3, pp. 253-261, May 1972.

[15] L. Chen and D.J.Edwards, "Applications of non-uniform sampling techniques and fast fourier transforms in plane near field antenna measurements", Proc. 8th Int. Conf. on Antennas and Propagation, Edinburgh, U.K., pp. 311-314, 1993.

[16] Mark S. Gatti and Yahya Rahmat-Samii, "FFT applications to plane-polar near-field antenna measurements", IEEE Trans. on Antenna and propagation, Vol. 36, No. 6, pp. 781-791, June 1988.

[17] Edward B. Joy, "Near-field range qualification methodology", IEEE Trans. on antenna and propagation, Vol. 36, No. 6, pp. 836-844, June 1988.

[18] Thorkild B. Hansen, "Formulation of probe-corrected planar near-field scanning in the time domain", IEEE Trans. on Antenna and Propagation, Vol. 43, No. 6, June 1995

[19] Arthur D. Yaghjian, "Probe correction for near-field antenna measurements", in Proc. Antenna Application Symp., Univ. Illinois, Sept. 1984

[20] Constantine A. Balanis, "Antenna theory analysis and design", John Wiley & Sons, 1982.

[21] Michael H. Francis, Allen C. Newell, Kenneth R. Grimm, John Hoffman, and Helmut E. Schrank, "Comparison of ultralow-sidelobe-antenna far-field patterns using the planar-near-field method and the far-field method", IEEE Antenna and Propagation Magzaine, Vol. 37, No. 6, pp. 7-15, December 1995.

[22] "Model 360 Vector Network Analyzer system operation manual", Wiltron

[23] "Model 360 Vector Network Analyzer system GPIB programming manual", Wiltron

[24] Lloyd hefford, "A prototype planar scanner for near field measuring system", Engineering project 8800, MUN, April 1996.

[25] Robert E. Collin, "Antenna and radiowave propagation", McGraw-Hill, Inc., 1985.

[26] Dave Butt, S.A.Saoudy, "Development of an L/C band microstrip antenna for satellite synthetic aperture radar", NECEC'96, St. John's, NF, Canada, May 1996.

Appendix I: VNA Calibration

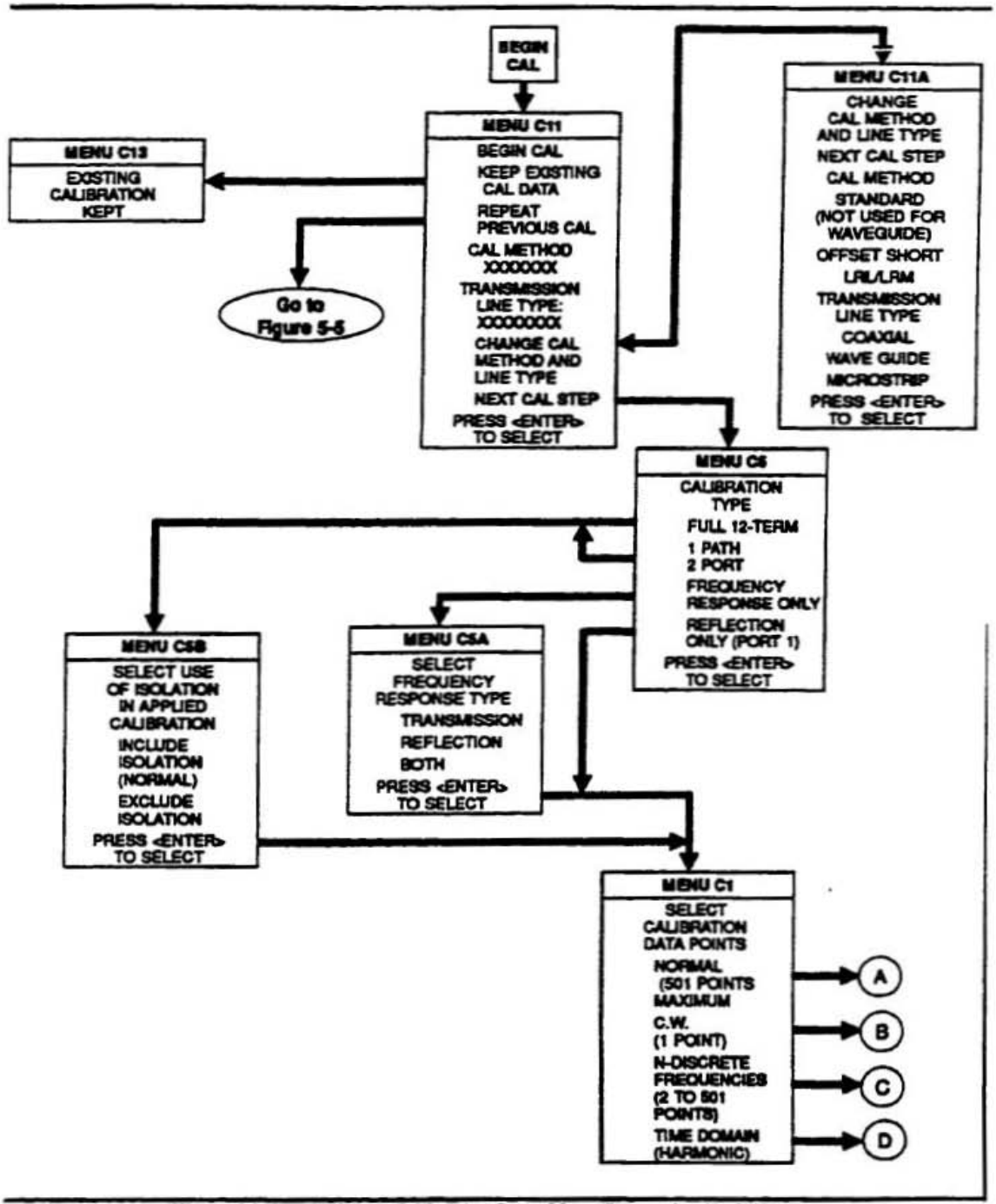

Figure 5-2. Standard OSL Calibration Setup Menu Sequencing (1 of 4)

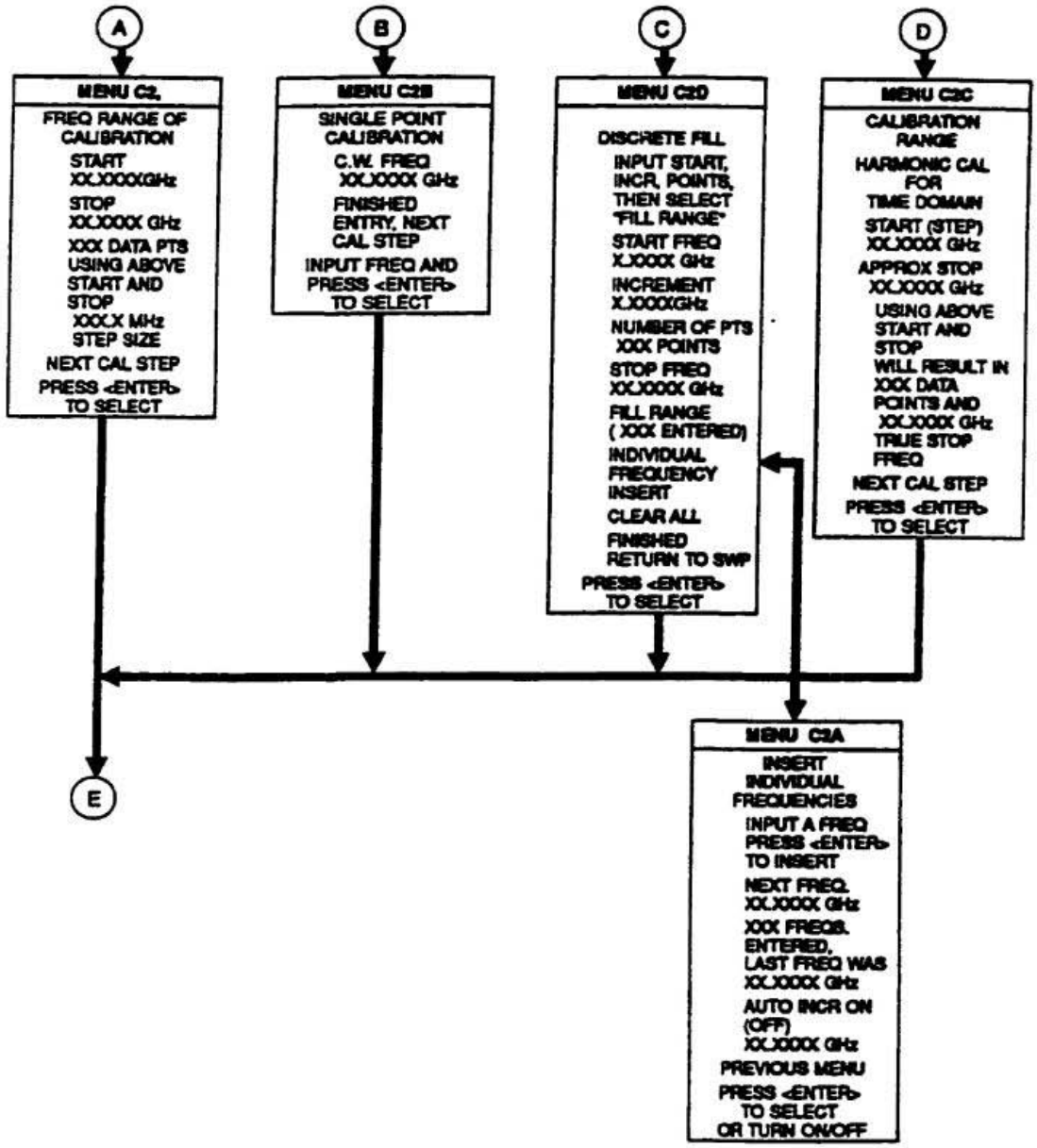

Figure 5-2. Standard OSL Calibration Setup Menu Sequencing (2 of 4)

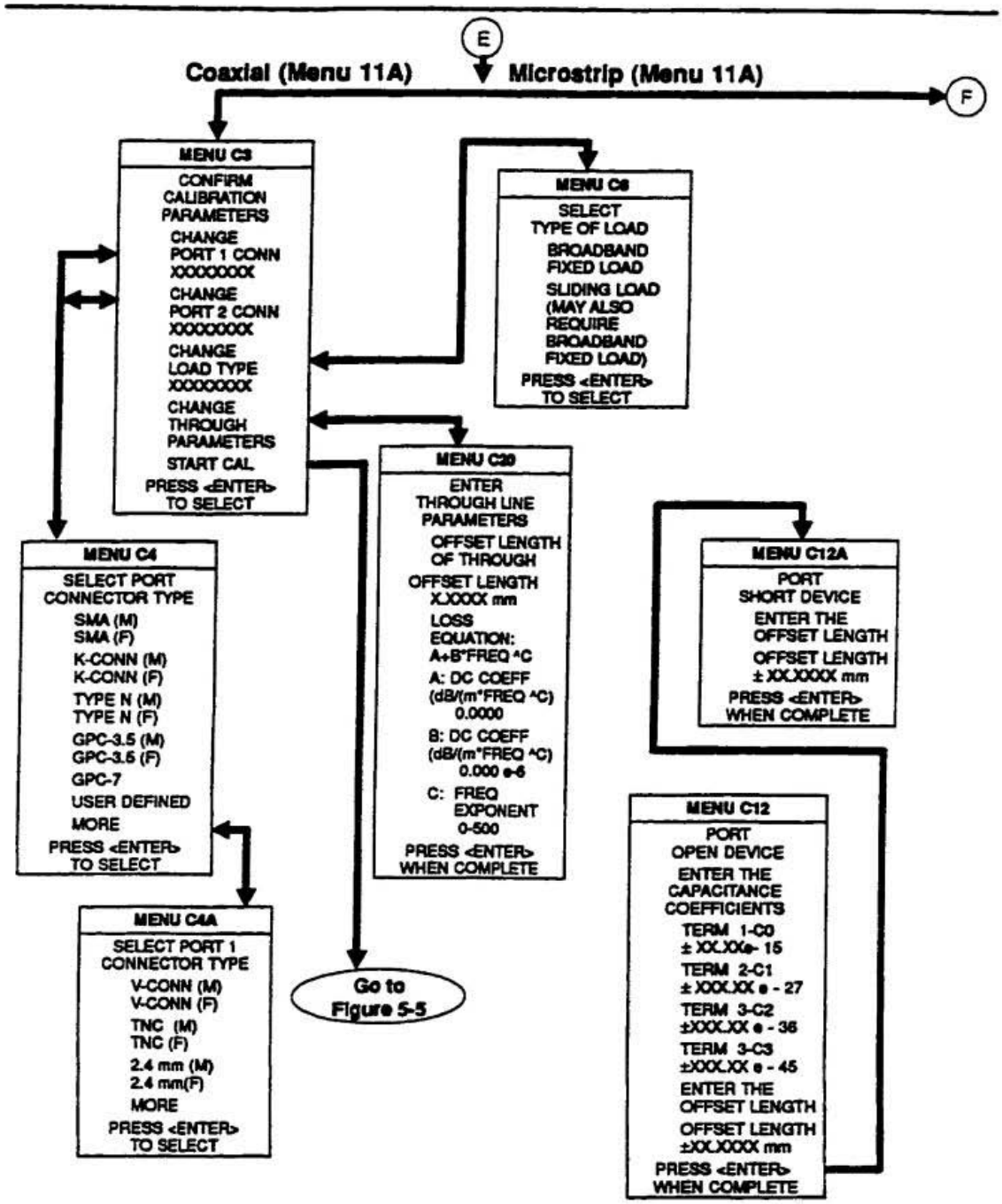

Figure 5-2. Standard OSL Calibration Setup Menu Sequencing (3 of 4)

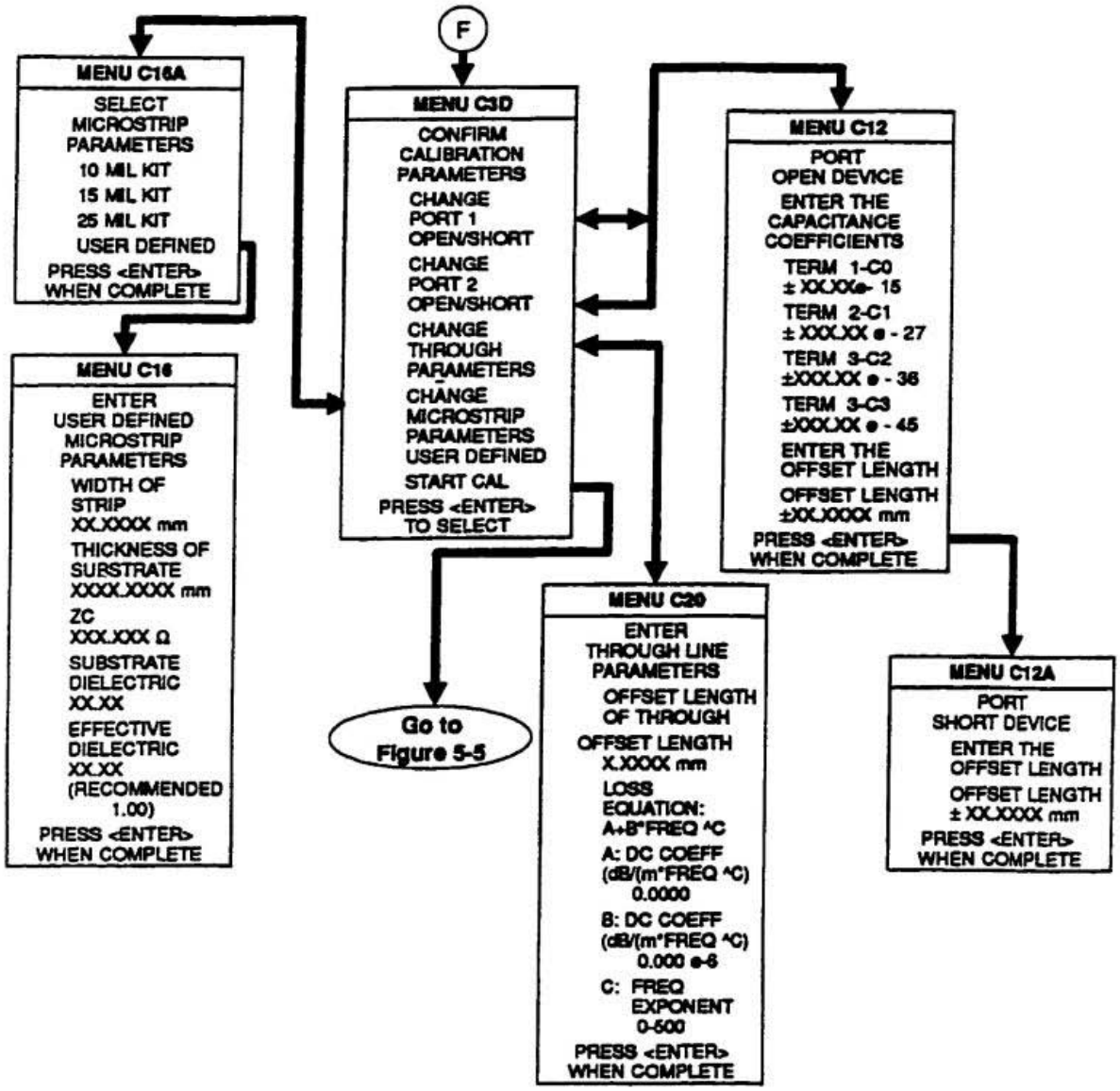

Figure 5-2. Standard OSL Calibration Setup Menu Sequencing (4 of 4)

Appendix II: GPIB Commands - Calibration

GPIB Command Group Function	Command Code Group
Calibration	A8T, A12, AFR, AFT, ARF, ARL, BBL, BEG, BPF C8T, C12, CC0 (value) thru CC3 (value), CF2, CF3, CFC, CFK, CFN, CFR, CFS, CFT, CFV, CM2, CM3, CMC, CMK, CMN, CMS, CMV, CND, CNG, COF, CON, COO (value), COS (value), CRF, CRL, CWC, DFC, DFD, DFQ (value), FIL, FRC, FRI (value), FRP (value), FRS (value), ISF, ISN, KEC, LCM, LL1 (value), LL2 (value), LL3 (value), LLZ (value), LM2, LM3, LR2, LR3, LTC, LTU, LTW, NCS, NOC, OCM, P1C, P2C, RGZ, RLZ, RM1, ROL (value), RPC, RRP, SBD (value), SBT (value), SCM, SH1 (value), SH2 (value), SLD, TCD, TDC, TDL, TFE, TFL, TOL, USE (value), USW (value), USZ (value), U10, U15, U25, WCO (value), WKD, WKI